

IMAGE LICENSED BY INGRAM PUBLISHING

Wideband Beamforming With Rainbow Beam Training Using Reconfigurable True-Time-Delay Arrays for Millimeter-Wave Wireless

Chung-Ching Lin, *Graduate Student Member, IEEE*, Veljko Boljanovic, *Graduate Student Member, IEEE*, Han Yan, *Graduate Student Member, IEEE*, Erfan Ghaderi, *Member, IEEE*, Mohammad Ali Mokri, *Graduate Student Member, IEEE*, Jayce Jeron Gaddis, *Student Member, IEEE*, Aditya Wadaskar, *Graduate Student Member, IEEE*, Chase Puglisi, *Member, IEEE*, Soumen Mohapatra, *Graduate Student Member, IEEE*, Qiuyan Xu, *Graduate Student Member, IEEE*, Sreeni Poolakkal, *Graduate Student Member, IEEE*, Deukhyoun Heo, *Senior Member, IEEE*, Subhanshu Gupta, *Senior Member, IEEE*, and Danijela Cabric, *Fellow, IEEE*

Abstract

The decadal research in integrated true-time-delay arrays have seen organic growth enabling realization of wideband beamformers for large arrays with wide aperture widths. This article

introduces highly reconfigurable delay elements implementable at analog or digital baseband that enables multiple Spatial Signal Processing (SSP) functions including wideband beamforming, wideband interference cancellation, and fast beam training. Details of the beam-training algorithm, system design considerations, system architecture and circuits with large delay range-to-resolution ratios are presented leveraging integrated delay compensation techniques. The article lays out the framework for true-time-delay

Digital Object Identifier 10.1109/MCAS.2022.3214408

Date of current version: 13 January 2023

based arrays in next-generation network infrastructure supporting 3D beam training in planar arrays, low latency massive multiple access, and emerging wireless communications standards.

I. Introduction

WIRELESS networks have fueled socio-economic growth worldwide and are expected to further advance to enable new applications such as autonomous vehicles, virtual and augmented reality, and smart cities. Due to shortage of sub-6 GHz spectrum, millimeter-wave (mmW) frequencies play an important role in the fifth generation (5G) communication networks. Recent research and development of 5G mmW networks has revealed that the propagation loss in the mmW band [1] needs to be compensated by antenna array gain [2] and densification of base stations with cell radius as small as a hundred meters [3], [4]. To make radio chipsets power and cost-efficient, state of the art (SOTA) 5G mmW transceivers are designed with phased antenna array (PAA) based subarray architecture [5], [6]. As a consequence, signal processing techniques [7] and network protocols [8] for 5GmmW networks are designed under constraints of PAA architectures.

Future generations of mmW networks will operate in the upper mmW frequency band where more than 10GHz bandwidth can be used to meet the ever-increasing demands [9], [10]. Their realization will demand addressing a completely new set of challenges including wider bandwidths, larger antenna array size, and higher cell density at the physical infrastructure level as highlighted in Fig. 1. These new system requirements demand fundamental rethinking of radio architectures, signal processing and networking protocols. Major breakthroughs are thus required in radio front-end architectures to enable wideband mmW networks, as most commonly adopted PAA based radios face many challenges in meeting the demanding requirements for different SSP functions.

A large portion of PAA implementations approximate the inter-element delay between the received signals with a phaseshift and hence the spatial processing is performed based on the phase difference between the received signals. This approximation simplifies the physical integrated circuit implementation, as compensating a phase shift is much simpler than a time delay. However, this simplification and approximation comes at the cost of limited operating fractional bandwidth of the receiver and will be analyzed further in Section II.

This article brings forward advances in true-time-delay (TTD) arrays that have the potential to significantly impact SSP for emerging wireless communication standards. We use TTD-based PAA [11]–[26] to first establish a contrast with the current phase shift only PAAs [27]–[46] that will be used for both data communications and direction finding. The application of TTD-based PAAs for different SSP functions will have ramifications for future mmW network infrastructure and emerging wireless standards. We next develop a TTDbased PAA exploiting the so called beam squint phenomenon to achieve precision direction finding overcoming fundamental latency bottlenecks in earlier beam training methods.

II. Exploiting Delay Compensation in Spatial Signal Processors

PAA operating over a very wide frequency band exhibits frequency-dependent beam pattern in an uncontrollable manner and it often degrades beamforming gain and directionality of the beam. This phenomenon is referred as spatial wideband effect [47] or beam squint [48]–[50], that becomes more significant in large antenna arrays.

This section will describe recent advances in SSP algorithms and architectures leveraging delay compensating circuits to overcome fundamental limits in analog PAAs. Interested readers are referred to [51] for a similar analysis for hybrid TTD PAAs. We will describe application of TTD arrays to realize different SSP modes when the array is used for data communications or for direction finding. In the former SSP mode, the TTD array will alleviate beam squint effects while in the latter

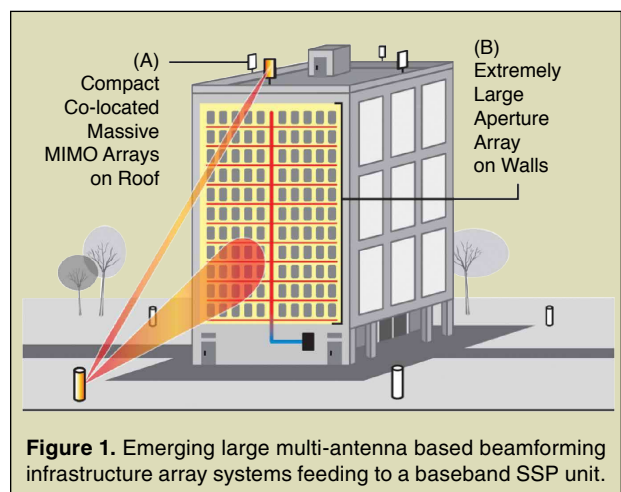


Figure 1. Emerging large multi-antenna based beamforming infrastructure array systems feeding to a baseband SSP unit.

Chung-Ching Lin, Erfan Ghaderi*, Mohammad Ali Mokri, Jayce Jeron Gaddis*, Chase Puglisi*, Soumen Mohapatra, Qiuyan Xu, Sreeni Poolakkal, Deukhyoun Heo, and Subhanshu Gupta are with the School of Electrical Engineering and Computer Science, Washington State University, Pullman, WA 99164 USA (e-mail: chung-ching.lin@wsu.edu). (*-work performed at Washington State University)
Veljko Boljanovic, Han Yan, Aditya Wadaskar, and Danijela Cabric are with the Department of Electrical and Computer Engineering, University of California at Los Angeles, Los Angeles, CA 90095 USA (e-mail: vboljanovic@ucla.edu).

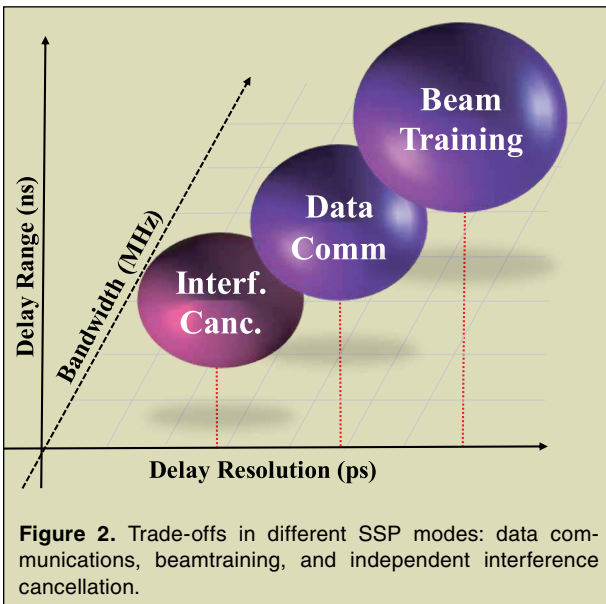
mode, intentional beam squint is introduced to achieve accurate but fast beam-training significantly reducing the search latency in existing analog PAAs. To realize these different SSP modes in a TTD PAA, it is important to understand the trade-offs between the delay range, delay resolution, and modulated bandwidth as shown in Fig. 2. Higher delay resolutions and moderate bandwidth are needed for beamnulling (independent interference cancellation [52]) whereas large delay range, moderate resolution, and large bandwidths are needed for beam-training. The SSP mode for independent interference cancellation is a corollary of the beamforming SSP and thus will not be studied in this article.

A. Mitigating Beam-Squint for Data Communications Mode

To alleviate the beam squint effect, the PAA is required to compensate inter-element signal delays before any SSP is done as illustrated in Fig. 3. Assuming a half-wavelength antenna spacing, the delay difference between the received signals in two consecutive antennas ΔT can thus be modeled as $\Delta T = d \sin(\theta) / c$, which can be also expressed as a frequencydependent phase shift difference $\Delta\Phi$ in the frequency domain through the following expression:

$$\Delta\Phi = 2\pi f \Delta T = \pi \sin(\theta) \frac{f}{f_c} \quad (1)$$

where f is frequency. If the signal of interest is narrowband, i.e., $f / f_c \approx 1$, the required TTD element can be replaced with a frequency-flat phase shifter (PS). This approximation is the basis of large portion of the SOTA SSP systems [19], [27][45]. A generalized implementation of phase shifting based SSP unit is shown in Fig. 4.



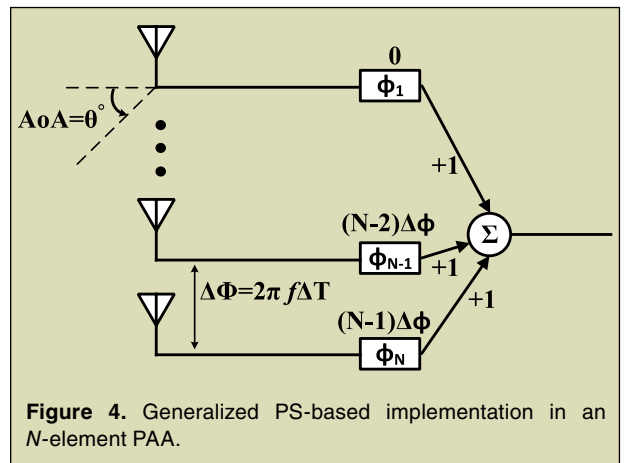
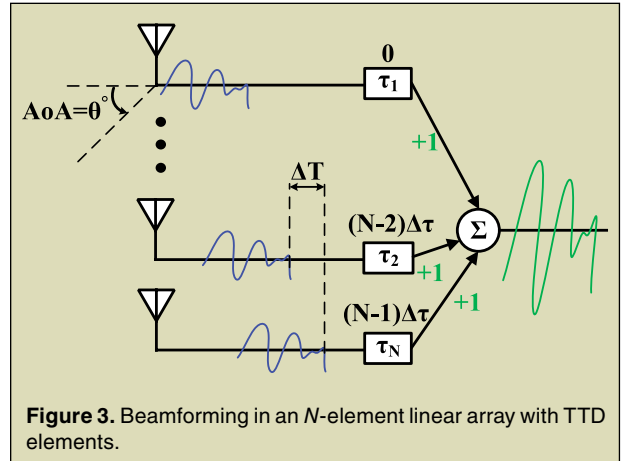
As for any approximation, replacing a TTD element with a PS imposes performance limitations. These limitations can be described both in the angular domain and the frequency domain. In the angular domain, PS-based implementation causes the intended angle-of-arrival (AoA) to be frequencydependent. To be more specific, the intended AoA, for the both beamforming and beam-nulling cases, varies with the signal of interest frequency as in:

$$\theta = \sin^{-1}\left(\frac{f_c \Delta\Phi}{f \pi}\right) \quad (2)$$

At the center frequency of the band, the PS-based and the TTD-based AoAs are the same and the beam is formed/nulled. As the frequency moves away from the center, the approximation of TTD with a PS becomes less valid and there will be an error between the actual and real intended AoA. This error can be formulated as follows:

$$\Delta\theta = \left| \sin^{-1}\left(\frac{f_c \Delta\Phi}{f \pi}\right) - \sin^{-1}\left(\frac{\Delta\Phi}{\pi}\right) \right| \quad (3)$$

This error depends on the actual AoA and the relative frequency of the interest. The maximum error happens



at the edges of the frequency band, as the frequency deviates the most from the center frequency. As the error is inversely proportional to the frequency, at the lower side of the frequency band error will be larger than the higher side of the band and this maximum error can be found as:

$$\Delta\theta_{\max} = \left| \sin^{-1}\left(\frac{f_c}{f_c - BW/2} \frac{\Delta\Phi}{\pi}\right) - \sin^{-1}\left(\frac{\Delta\Phi}{\pi}\right) \right| \quad (4)$$

where BW is the signal bandwidth and BW/f_c is called the fractional bandwidth. In Fig. 5, the maximum error in the angular domain for a PS-based SSP unit is plotted versus the ideal intended AoA, for three cases of fractional bandwidths. In this plot the AoA range is limited to $\pm 60^\circ$, since for larger AoAs the actual AoA can be as high as $\pm 90^\circ$ and the error in those cases does not reflect the severity of the PS-based implementation. As it can be seen, this error can get as high as 22° which results in non-alignment with the intended transmitter and consequently loss in the desired signal (beamforming case) or imperfect cancellation (beam-nulling case). The frequency-dependent approximation of a TTD element with a PS results in frequency-dependent beamforming gain that acts as a bandpass filter [20], [22], and imperfect frequency-dependent beam-nulling that results in wideband interference leakage [23], [52].

The beamforming gain in a PS-based N -element receiver can be modeled as the absolute value of the inner product $G(f) = |\mathbf{w}^H \mathbf{a}|$, where \mathbf{w} is a receive beamformer and \mathbf{a} is a spatial response vector. Assuming a phase difference of $\Delta\phi$ between neighboring PSs, the n -th element of \mathbf{w} is defined as $[\mathbf{w}]_n = \exp(-j(n-1)\Delta\phi)$. On the other hand, using (1), the n -th element of \mathbf{a} is defined as $[\mathbf{a}]_n = \exp(-j(n-1)\Delta\Phi)$. Expressed as a sum of complex exponentials, the gain $G(f)$ becomes

$$G(f) = \left| \sum_{n=1}^N e^{j(n-1)(\Delta\phi - \Delta\Phi)} \right| \quad (5)$$

In Fig. 6, the normalized beamforming gain $G(f)/N$ for intended AoA of 45° versus normalized frequency f/f_c of the input signal for three cases of $N = 4, 16, 64$, are plotted. The beamforming gain in a PS-based implementation acts as bandpass filter for the desired signal. Similar to a filter, the 3-dB fractional bandwidth ($FBW_{3\text{ dB}}$) can be defined as the fractional bandwidth where the beamforming gain drops 3 dB compared to the maximum value (N). As proven in [53], [54], for large values of N , the $FBW_{3\text{ dB}}$ is given as:

$$FBW_{3\text{ dB}} \cong \frac{1.772}{N|\sin(\theta)|} \quad (6)$$

For larger arrays $FBW_{3\text{ dB}}$ becomes smaller and the approximation of a TTD element with a PS becomes less valid. Similar to the outcome of the beam squinting error, as the intended AoA increases, the $FBW_{3\text{ dB}}$ gets smaller and the effective error increases.

B. Beam-Squint for Beam-Training Mode

Beam-training is a part of the initial access (IA) protocol in mmW networks that has a goal to align the beamforming directions and realize the maximum gain between the base station (BS) and user equipment (UE) [55], [56]. The majority of existing mmW beam-training algorithms was designed for PAAs which frequency-flat PS in all antenna branches to steer/combine the signal in a desired direction. With a single mmW chain, power-efficient analog PAAs can synthesize only one spatial beam with all frequency components being aligned in the same direction, as illustrated in Figure 7(a). Thus, the existing beam-training schemes with analog PAAs include various types of exhaustive beam sweeping where different beam candidates are sequentially probed to find the dominant AoA or angle-of-departure (AoD) [57]-[60]. The required number of probing beams linearly

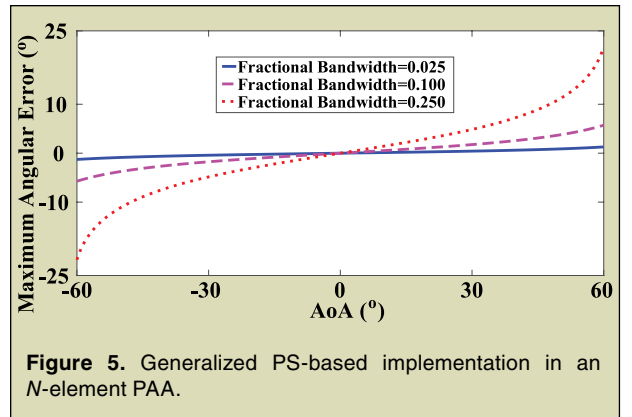


Figure 5. Generalized PS-based implementation in an N -element PAA.

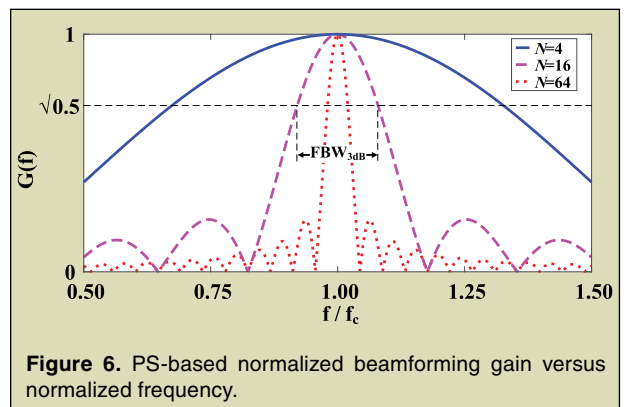


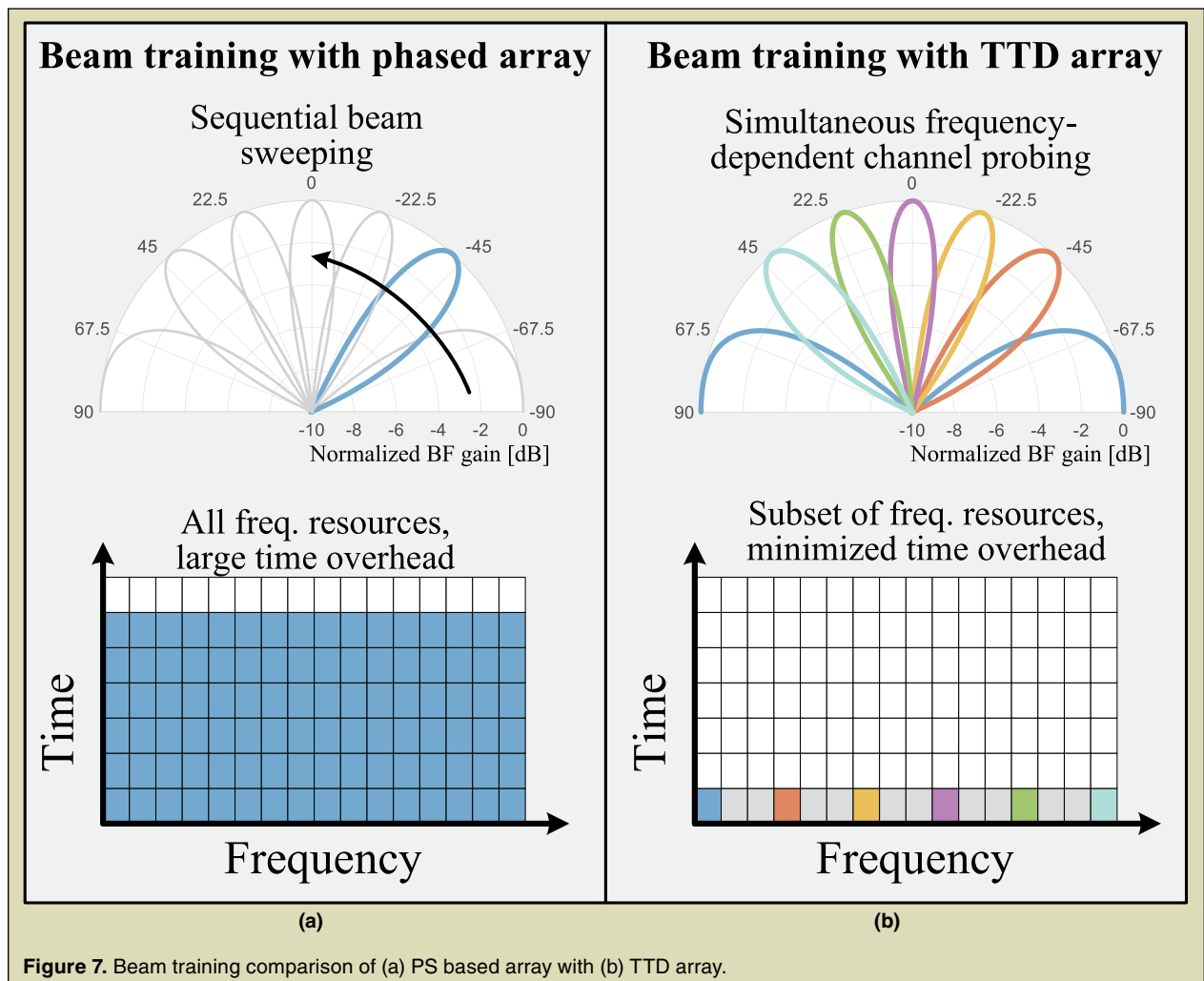
Figure 6. PS-based normalized beamforming gain versus normalized frequency.

scales with the number of antenna elements N , thus, the beam-training overhead becomes a bottleneck for low-latency communications. Sub-array based PAAs with N_{RF} RF chains can reduce the overhead by probing N_{RF} beams simultaneously. However, since $N_{\text{RF}} < N$, they need to rotate the N_{RF} beams in consecutive training symbols to cover all angular directions. Besides a lower beamforming gain for each beam, sub-array based PAAs also come at the cost of a higher power consumption due to the presence of N_{RF} radio frequency (RF) chains. SOTA IA approaches based on 5G requirements are limited to narrowband pilots and relatively small antenna arrays, so the latency of PAA-based IA is acceptable. However, the future evolution of mmW-nets will be IA latency limited and it would require the use of wideband pilots and new radio architectures that can probe a large number of AoAs/AoDs in parallel as illustrated in Figure 7(b).

To address this fundamental issue in mmW PAAs, this article will introduce a fast beam training

method leveraging TTD arrays. Instead of suppressing the beam squint effect evident in mmW arrays, we will exploit this effect to our advantage by introducing intentionally large time delays in each antenna branch to realize frequency-dependent probing beams which can be exploited to accelerate the channel probing capability. These frequency-dependent beams will be fully controlled by adjusting the delay introduced in TTD circuits [61]. In addition, the number of simultaneously probed frequency-dependent beams in TTD arrays can be rather large, even when there is only one RF chain. These features give an advantage to TTD arrays over conventional sub-arrays based PAAs for fast and power-efficient beam-training.

In summary, this article presents reconfigurable delay compensating circuits with large delay range and bandwidth, and finer delay resolution to realize wide-band mmWSSP. Section III summarizes the TTD SSP architectures highlighting the challenges associated



with realizing large delay compensation with fine resolution at different domains in the receiver chain. Section IV discusses the fast beam-training algorithm and practical design considerations for analog PAAs leveraging TTD SSP architecture. Section V will present the hardware implementation of reconfigurable time delay units enabling different SSP modes along with hardware validation methods for wideband PAAs. Section VI presents future works expanding the proposed TTD-based PAAs for beam-training with planar arrays, multiple access applications, and standardization of wireless protocols. Section VII concludes this article.

III. Overview of mmW TTD PAAs

This section describes the possible architectural choices for TTD PAAs. The design of PAAs are based on two principles: (1) phase/delay alignment of signals either in transmit or receive path, and (2) summation of phase/delay aligned signals. To align the received signals in a PAA, delay elements should provide the proper delay to each received signal. The delay can be applied to the signal in mmW, LO, baseband, or digital domains. When the fractional bandwidth of the signal or the required delay range in the phased array system is small, the delay is approximated by a phase shift as discussed before. There are different topologies that are common in the implementation of PAA transceivers (Fig. 8) such as RF phase shifting [62]-[65], LO phase shifting [66], [67], baseband (BB) phase shifting [68], [69], and digital phase shifting [70]. In the RF phase-shifting architecture, after applying the required phase shift in each RF path, the signals can be combined together. LO phase shifting architecture uses the PS in the LO port of the mixer. In BB and digital phase-shifting architecture, the received signals are aligned after downconversion, using analog circuitry in baseband or in a digital processor. Either of these architectures is a good candidate when the signal's fractional bandwidth is small, or the required delay range in the PAA is small.

For large delay-bandwidth product cases, delay units are necessary to prevent beam squint. Similar to a PS-based PAAs, the location of the time delay unit makes possible multiple architectures (mmW/RF path, LO port of the mixer, BB, or digital domains). In the mmW/RF TTD architecture, the time delay unit is placed in the mmW/RF domain before downconversion. The received signals at each receiver path can be combined constructively, as shown in Fig. 8(a). The mixer is shared between multiple paths and only one LO signal is necessary which allows significant area and power reduction. As the signals are combined before

downconversion, interferers are removed due to spatial filtering, which reduces the linearity requirements of the blocks after the combiner. Although there are different implementations of the mmW/RF TTD-based PAAs, these implementations occupy a large area on the chip and there are serious limitations on the delay range. Table 1 highlights the integrated mmW/RF TTD implementations over the past decade starting with the seminal work [71] by Chu and Hashemi in 2007. Placing the TTD element in the LO path of the mixer does not resolve these limitations especially when handling wideband range. One may wonder whether it's possible to place TTD block in the LO path. Since the LO signal is a single tone, the time delay can be replaced as a phase shift which can further be moved to either RF, or BB side mathematically. However, this scenario is identical to compensating a wideband signal using the phase shift, eventually, introducing beam squint at band edges. Therefore, the LO TTD approach does not resolve these limitations when handling wideband range. Digital TTD PAA is the same as a digital phased array and the challenges are the same such as high power consumption including the need for highly linear analog-to-digital converter (ADC) as well as other linear elements. However, there are promising TTD-based PAAs in BB with large delay-bandwidth products [22], [72]. Table 2 highlights recent SOTA TTD-based PAAs and delay lines implemented at BB.

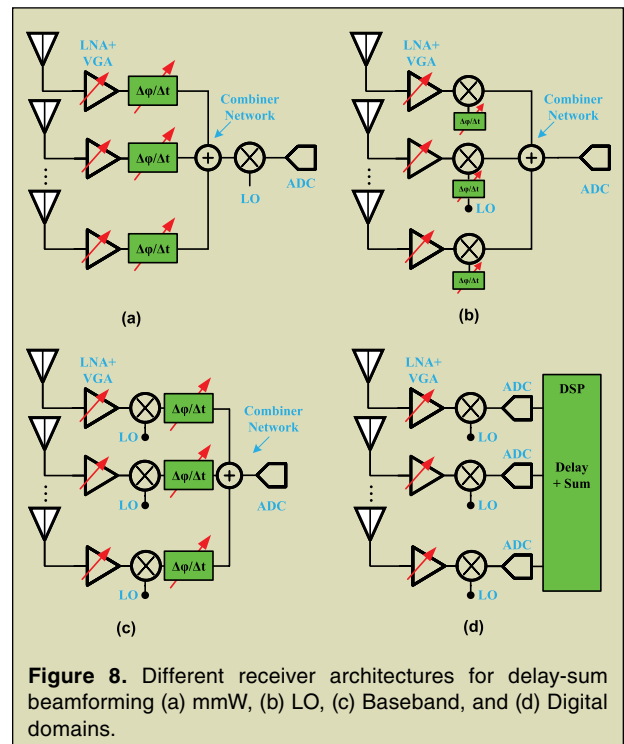


Figure 8. Different receiver architectures for delay-sum beamforming (a) mmW, (b) LO, (c) Baseband, and (d) Digital domains.

In an array with BB TTD elements as shown in Fig. 9 [22], instead of delaying the down-converted and phase shifted signals from the antennas followed by sampling and digitization, the signals are sampled at different time instants. Thus, the complexity of delaying signals is shifted to the clock path where precise and calibrated delays can be applied in the advanced semiconductor technology nodes. More importantly, a large delay range-to-resolution ratio can be easily realized while supporting a relatively larger number of antennas and bandwidth. The switched-capacitor adder based implementation requires multiple time-interleaved and delay compensated phases for formation of the beam [22]. In the sampling phase, the input signal from each channel is first sampled (with delayed time-interleaved clocks) on a sampling capacitor. After the last sampling phase, the stored charges on each capacitor corresponding to each channel (and each timeinterleaved phase) are summed to form the beam. However, since time delay in BB is not mathematically equivalent to the time delay in the RF domain, a small phase shift is still necessary [20], [22]. For example, if a time delay of τ_d is needed, it can be implemented in the BB with a time delay equal to τ_d plus a phase shift equal to $-\omega_{LO}\tau_d$ [20], [22], [37]. The BB TTD architecture shown in Fig. 9 is hereby referred as discrete-time TTD SSP.

A PS can be implemented in the RF, LO, BB, or digital domain to provide the required phase shift to the BB time delay units. The mmW/RF PS can be limited by the maximum delay-bandwidth product of the receiver.

Digital implementation of the TTD or PS is similar to digital phaseshifting architecture with each RF path requiring an ADC which increases the power consumption of the whole system considerably. ADCs should be linear enough to tolerate the large interferences which further increases the whole system's power consumption. Placing a PS in BB or LO is another feasible option (Fig. 9). In these architectures, each RF path has a dedicated mixer and an LO signal. PS in the LO port of the mixer should operate at the LO frequency. However, the PS in the BB or intermediate frequencies has to operate at lower frequencies. Though the loss and phase error of the PS in RF frequencies is higher than the PS at BB, the PS at the BB has to operate at a much higher fractional bandwidth while the PS in LO path only deals with a single tone signal (Fig. 9(a)). The PS can be implemented in the LO [73] as well as conventional PS architectures.

BB PS using vector summation is also another option. Vector summing PS is based on the weighted summation of quadrature signals. Quadrature signal generation is possible using a quadrature coupler, polyphase filters, or using quadrature mixers. Quadrature couplers at the BB occupies a large chip area and thus less preferred. Polyphase filters usually are narrow-band which contradicts with the large-delay bandwidth required. The use of quadrature downconversion mixers is another option though at the expense of routing complexities.

The next section presents the framework of leveraging discrete-time TTD SSP for fast beam-training

Table 1.
Survey of TTD implementations at RF/mmW.

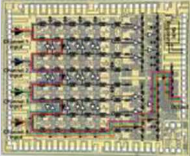
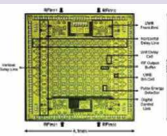
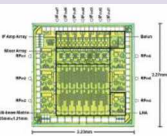

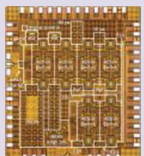
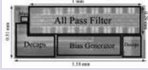
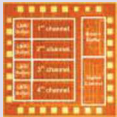
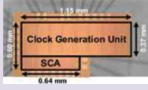

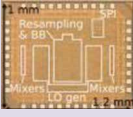
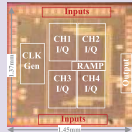
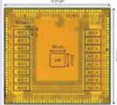
	 JSSCC'07 [12]	 COMM'08 [13]	 TMTT'13 [14]	 IMS'15 [16]	 RFIC'18 [17]
TTD Method	LC Delay	LC Delay	LC Delay	LC Delay	LC Delay
# of FE Elements	4	2 × 2	6	-	-
# of Beams	1	49	7	-	-
Domain	RF	RF	RF	RF	RF
Freq.(GHz)	8	8	35	1~20	2~20
Bandwidth (MHz)	18000	15000	10000	19000	18000
Delay Range/Resolution (ps)	300/15	1750/150	/10	400/5	508/4
Area (mm ²)	9.9	16.8	5.1	4	5.45
Power (mW)	560	945	825	6	285
IC technology	CMOS (130)	CMOS (130)	BiCMOS (130)	CMOS (130)	BiCMOS (130)

Table 2.
Survey of TTD implementations at BB.

	 JSSC'17 [19]	 JSSC'15 [15]	 TCAS-1'19 [22]	 ISSCC'20 [23]	 SSCL'20 [24]	 ESSCIRC'21 [26]	 JSSC'20 [20]
Method	CT (Gm-C)	CT (Gm-C)	DT (Swit Cap)	DT (Swit Cap)	DT (Swit Cap)	DT (Swit Cap)	Digital BB
Arch.	-	MISO	MIMO	MISO	MISO	MISO	MIMO
# FE elements	-	4	4	4	4	4	16
Domain	Voltage	Voltage	Charge	Time	Charge	Charge	Digital
Combiner	-	OTA	OTA	VTC ^a	Passive	OTA	Adder
Freq. (GHz)	-	1~2.5	0~0.1	1.25~1.75	0.6~4	28	1
BW (MHz)	2000	1500	100	500	800	800	100
Delay Range (ns)	1.7	0.55	15	1	5	3.8	7.5
Resolution (ns)	0.01	0.013	0.005	0.015	0.035	0.003	0.25
Area (mm ²)	0.6	0.07	0.57	0.31	0.13 ^c	1.98	0.29 ^d
Power (mW)	112-364	360	47 ^b	40	122 ^c	29	453
IC tech. (nm)	CMOS (130)	CMOS (140)	CMOS (65)	CMOS (65)	CMOS (28)	CMOS (65)	CMOS (40)

^a Series beamforming. ^b includes non-uniform sampling generator. ^c includes 4-element RF front-end. ^d without pads.

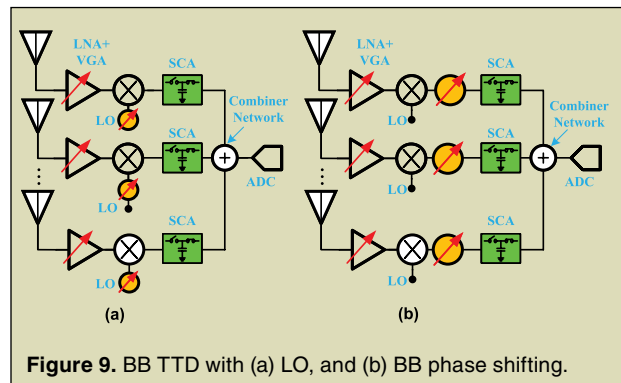
followed by details on hardware implementation and experimental validation of TTD SSP.

IV. Rainbow Beam-Training Using Discrete-Time TTD SSP

This section describes the design of TTD array parameters, which enable a training codebook of frequency-dependent beams to be synthesized. We also explain the corresponding frequency-domain digital signal processing (DSP) algorithm [61]. We further discuss the practical aspects of TTD beam training including the sensitivity to hardware impairments, power allocation and the peak-to-average power ratio (PAPR) problem in orthogonal frequency-division multiplexing (OFDM) systems, and achievable beam training distance.

A. Introduction to Rainbow Beam-Training for mmW PAAs

Recent work on mmW and sub-THz beam-training has been focused on minimizing the required overhead using frequency-dependent beam steering/combining [13], [51], [61], [74], [76]. The main idea is to leverage different antenna architectures that can synthesize



rainbow beams to probe the entire angular range simultaneously. Each rainbow beam is associated with a different frequency, thus, information of the best steering/combining direction is embedded in the signal spectrum and it can be obtained through simple frequencydomain DSP. In [74], the authors proposed to use leaky wave antenna (LWA) for a single-shot AoA estimation. In [75], a delay-phase array architecture was proposed for fast beam tracking with rainbow beams at THz frequencies. TTD array architectures in [13] implemented delay elements in

RF, which are known to suffer from low scalability in terms of required area and power efficiency when the array size becomes large. In our recent work in [51], [61], [76], we proposed a scalable TTD array with delay elements implemented in baseband for a single-symbol mmW beam training in an OFDM system. The key idea was to exploit signal delaying in each antenna branch to exacerbate the wideband spatial effect (beam squint) among subcarriers in a controllable manner, i.e., to create a frequency-dependent codebook which probes all angular directions at once. This is achieved by properly configuring the delay and phase taps in a TTD array.

B. TTD Codebook and DSP Algorithm Aesign

In our recent work we introduced TTD-based beam-training at the UE side that requires only one OFDM symbol [51], [61], [76]. We assume that the BS with N_T antennas uses a fixed frequency-flat precoder $\mathbf{v} \in \mathbb{C}^{N_T}$ designed according to the previously estimated AoD. The received signal $Y[m]$ at the m -th OFDM subcarrier can be expressed as follows

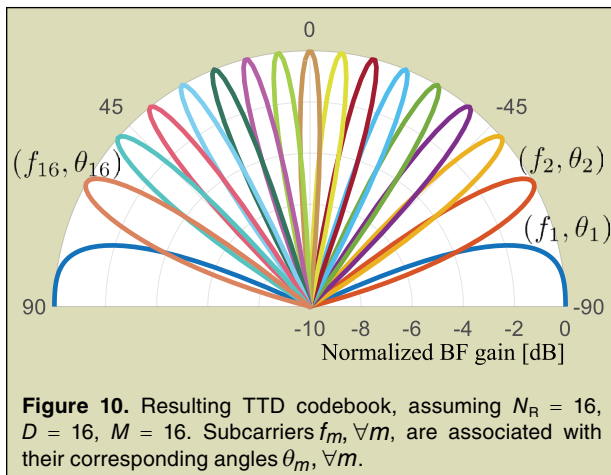
$$Y[m] = \mathbf{w}^H[m] \mathbf{H}[m] \mathbf{v} s[m] + \mathbf{w}^H[m] \mathbf{n}[m], \quad (7)$$

where $\mathbf{w}[m] \in \mathbb{C}^{N_R}$ is a frequency-dependent UE TTD combiner, $\mathbf{H}[m] \in \mathbb{C}^{N_R \times N_T}$ is a channel matrix, $s[m]$ is a pilot, and $\mathbf{n}[m] \sim \mathcal{CN}(0, \sigma_n^2 \mathbf{I}_R)$ is a noise vector at the m -th subcarrier, respectively. The n -th element of \mathbf{w} is defined as

$$[\mathbf{w}[m]]_n = \alpha_n \exp(-j(2\pi(f_m - f_c)\tau_n + \phi_n)). \quad (8)$$

where $\alpha_n = 1$, τ_n , and ϕ_n are the gain, delay tap, and phase tap in the n -th antenna branch, respectively.

Assuming the bandwidth BW and a uniform linear array (ULA) with a frequency-flat spatial response at the



UE side, it was shown in [61] that a codebook of rainbow beams which cover the entire angular range $[-\pi/2, \pi/2]$ can be created by setting the delay taps $\tau_n, \forall n$, as follows

$$\tau_n = (n-1)\Delta\tau, \forall n, \text{ where } \Delta\tau = 1/\text{BW}, \quad (9)$$

Since the taps in (9) are proportional to the Nyquist sampling period, the codebook can be obtained without the need to implement a fractional ADC sampling. In such a codebook, the rainbow beam associated with the subcarrier frequency f_m is pointing in the angle θ_m given as follows [61]

$$\theta_m = \sin^{-1}(\text{mod}(2f_m\Delta\tau + 1, 2) - 1). \quad (10)$$

An example of the resulting TTD codebook for a UE with $N_R = 16$ antenna elements is provided in Fig. 10. To probe $D = N_R = 16$ directions, $M = 16$ subcarriers need to be used. The codebook can be designed to be more robust in frequency-selective channels by mapping R different subcarriers to each probed direction. This is achieved by increasing the delay difference between antenna elements R times, i.e., $\Delta\tau = R/\text{BW}$ [76]. With R being the codebook diversity order and R the number of probed directions, TTD beam training requires a waveform with $M = DR$ loaded subcarriers.

The pointing angles $\theta_m, \forall m$, of rainbow beams can be jointly rotated by using the frequency-flat PSs in the TTD array. A rotation of θ_{rot} requires the phase taps $\phi_n, \forall n$, to be set as follows

$$\phi_n = (n-1)\Delta\phi, \forall n, \text{ where } \Delta\phi = \pi \sin(\theta_{\text{rot}}). \quad (11)$$

The rotated angles can then be expressed as $\theta'_m = \theta_m + \theta_{\text{rot}}, \forall m$.

With this codebook and described frequency-to-angle mapping, the information of the dominant propagation angle can be acquired with simple frequency-domain DSP. Given the received signal in (7), a coarse AoA estimate $\hat{\theta}$ is given as $\hat{\theta} = \theta_{m^*}'$, where the angle θ_{m^*}' corresponds to the subcarrier with the strongest received signal power. Mathematically, the estimation can be expressed as

$$\hat{\theta} = \theta_{m^*}', \text{ where } m^* = \underset{m}{\text{argmax}} |Y[m]|^2. \quad (12)$$

If the codebook diversity is R , the power $|Y[m]|^2$ is averaged across all R subcarriers m mapped into the same direction before angle estimation.

The estimation accuracy can be improved by designing a high-resolution dictionary-based algorithm that relies on the codebook with diversity order R [76]. The average received signal power in all probed

directions can be correlated with an oversampled dictionary of UE beamforming gains to obtain an accurate angle estimate.

C. Practical Considerations in TTD Beam-Training

1. *Sensitivity to Hardware Impairments:* In practice, errors in different hardware components can distort the delay taps in (9) and phase taps in (11) and thus affect the designed beam training codebook. We assume that delay errors can be modeled as Gaussian random variables, such that the distorted taps are $\tilde{\tau}_n \sim N(\tau_n, \sigma_T^2)$, where σ_T^2 is the error variance. The phase errors occur due to imperfect PSs, LOs, imbalance between in-phase and quadrature-phase samples, or other hardware errors. Similarly as with the delays, we model the distorted phase taps as $\tilde{\phi}_n \sim N(\phi_n, \sigma_P^2)$, where σ_P^2 is the error variance. In addition to the phase and delay errors, we consider distorted gain $\tilde{\alpha}_n$ in all antennas branches. The gains are modeled with a log-normal distribution, i.e., $10\log_{10}(\tilde{\alpha}_n) \sim N(0, \sigma_A^2), \forall n$.

We have numerically evaluated the impact of all three hardware errors on the TTD beam training performance. Specifically, we compared the impact on two algorithms, including the coarse angle estimation algorithm introduced in the previous subsection and high-resolution algorithm in [76]. The assumed simulation parameters are summarized in Table 3. In Fig. 11, we study the impact of gain and phase errors on the root mean square error (RMSE) of AoA estimation, under no delay error. For both algorithms, severe performance degradation occurs when the standard deviation of the gain error $\sigma_A \geq 2.5$ dB and phase error $\sigma_P \geq 30^\circ$. In Fig. 12, the impact of TTD delay error is presented. With the proposed TDD architecture where time delay units are implemented in baseband, both algorithms are robust to delay errors with standard deviation of up to $\sigma_T = 125$ ps. In comparison, both algorithms start to show severe degradation with only $\sigma_T = 1.5$ ps in TDD architectures with RF time delay units studied in previous work [76]. This result indicates that both algorithms have more relaxed specifications for baseband implementation of TTD units compared to the RF TTD arrays.

2. *Power allocation and Supported Distances:* The proposed frequency-dependent beam-training uses an OFDM based waveform where only a subset of M out of M_{tot} ($M < M_{\text{tot}}$) subcarriers is loaded at the BS. This allows the transmit signal power

to be allocated to a lower number of subcarriers, which can increase the SNR per subcarrier compared to that in conventional beam-training, as illustrated in Fig. 13. Specifically, when the total transmit power P_T is divided among M subcarriers, the SNR per subcarrier is given by the following expression

$$\text{SNR}_{\text{sc}} = \frac{G_T G_R \lambda^2}{(4\pi d)^2} \frac{P_T}{\Delta \text{BW} N_0 M} \quad (13)$$

assuming a free-space path loss model. The terms $G_T = 20\log_{10}(N_T)$, $G_R = 20\log_{10}(N_R)$, λ , and d represent the transmit beamforming gain, receive beamforming gain, wavelength, and

Table 3.
Assumed parameters for numerical evaluation.

Symbol	Value	Description
f_c	60 GHz	Carrier frequency
BW_{tot}	2 GHz	Bandwidth
N_T	4096	Total number of subcarriers
N_R	128	Number of BS antennas
D	16	Number of UE antennas
R	32	Number of probed directions
$M (= DR)$	4	Codebook diversity order
Q	128	Number of used subcarriers
signal-to-noise ratio (SNR)	1024	Dictionary size in [76]

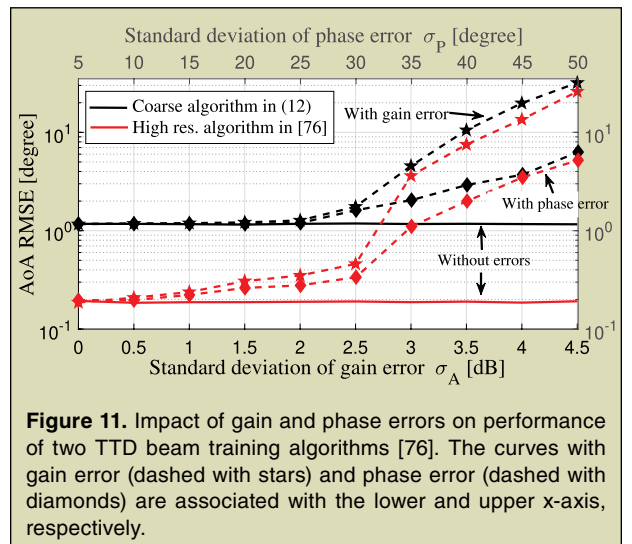


Figure 11. Impact of gain and phase errors on performance of two TTD beam training algorithms [76]. The curves with gain error (dashed with stars) and phase error (dashed with diamonds) are associated with the lower and upper x-axis, respectively.

distance between the BS and UE. Power spectral density of the noise is denoted as N_0 , while $\Delta\text{BW} = \Delta / (M_{\text{tot}} - 1)$ represents the subcarrier spacing. Note that the SNR per subcarrier is M_{tot}/M times larger than with a fully loaded OFDM waveform. Since the proposed DSP algorithm considers only M loaded subcarriers with high SNR, angle estimation in (12) is not noise-limited. Further, due to a lower number of used subcarriers, the proposed OFDM waveform for TTD beam training results in a more than 2 GB lower PAPR than a fully loaded OFDM waveform, as presented in Fig. 14, where we assumed the same simulation parameters as in the previous subsection. We used a cyclic prefix of 128 samples and assumed that subcarriers are loaded either with binary phase shift keying (BPSK) or quadrature phase shift keying (QPSK) symbols.

Although the proposed frequency-dependent beam-training can benefit from a higher SNR per subcarrier, the supported distances between the BS and UE are reduced compared to the PAA beam sweeping approach. This is because the UE has a lower total received signal power. Specifically, with the codebook in Fig. 10, which probes D different directions, roughly $1/D$ of the signal power is received per direction. The received signal power corresponds to the subcarriers that probe the

dominant AoA. To evaluate the impact of a lower received signal power on the beam-training performance, we compared the AoA RMSE of TTD-based algorithms and PAA-based beam sweeping at different distances between the BS and UE. We assumed a non-line-of-sight scenario and modeled the path loss according to mmMAGIC channel [77]. We considered two array sizes at the UE, including $N_R = 16$ and $N_R = 32$. With $N_R = 16$, $D = 32$ directions are probed, while with $N_R = 16$, $D = 32$ directions are probed. Other parameters are the same as in the previous subsection. The comparison results are presented in Fig. 15, where we highlighted the distances that the compared beam training algorithms can support. PAA-based beam sweeping combines the entire signal bandwidth in each probed direction and thus achieves a high received signal power and reliable angle estimation at different distances. Nevertheless, it requires large overheads of 32 and 64 OFDM symbols to do so when $N_R = 16$ and $N_R = 32$, respectively. Sub-array based PAAs can reduce the overhead by sweeping multiple beams at the same time, but this comes at the cost of a lower beamforming gain and thus a lower supported distance, as shown in Fig. 15 for 4 sub-arrays, i.e., 4 and 8 antenna elements per sub-array. TTD beam training algorithms are based on a single OFDM symbol and their angle estimation accuracy is comparable to that of exhaustive PAA beam sweeping. However, TTD-based algorithms have the smallest supported distances among the compared approaches. We note that with a more sophisticated detection algorithm that exploits the waveform structure, beam training capabilities and supported distances of TTD arrays could increase. We leave a more detailed theoretical study of supported distances and better detection algorithms for future work.

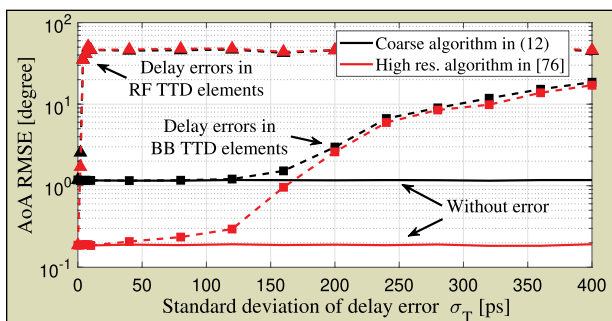


Figure 12. Impact of delay error on performance of two TTD beam training algorithms [76].

V. Reconfigurable Discrete-time TTD SSP Hardware Design Considerations

In this section, we describe the design and hardware implementation of reconfigurable time delay units in the

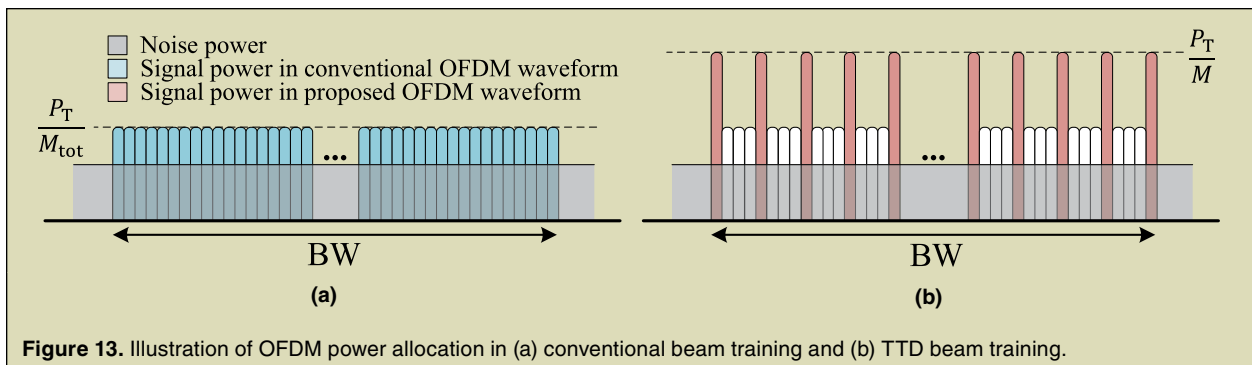


Figure 13. Illustration of OFDM power allocation in (a) conventional beam training and (b) TTD beam training.

discrete-time TTD SSP shown in Fig. 9 applied to both the data communications as well as beam-training SSP modes.

A. Important Sub-Systems in Discrete-Time TTD SSP

The analog array though more energy efficient when compared to hybrid TTD and digital arrays [51] require larger unity-gain bandwidth amplifiers to have similar performance. The circuit performance is further constrained with the parasitic capacitance, routing losses, crosstalk, and any possible mismatches during fabrication evident at multiple levels including silicon, packaging, or printed circuit board. Design considerations for the key blocks are described here to ensure low-power consumption is upheld for analog arrays as compared to hybrid or digital TTD SSP [51] including its ability to achieve fractional delays with high precision. This section presents design considerations for the key design blocks: (i) sample-and-hold, (ii) wideband signal combiners, and (iii) precision clock generation. Fig. 16 shows a more detailed illustration of the discrete-time TTD SSP. The circuit design consideration to support rainbow beam training lies in determining the minimum number of interleaving level that is required to achieve a certain delay. For a critically spaced linear N element array, $\lambda/2$ spacing, and an antenna system with a diversity factor of unity, we derive the minimum interleaving level, denoted as M_{BT} , and express as:

$$M_{BT} \geq 1 + 2(N - 1) \quad (14)$$

As observed, the required levels increase linearly with the number of antennas, leading to the inclusion of more samplers which comprise of high linearity switches and capacitors in the design. Interested readers can refer to [22], [26], [51], [52] for further understanding.

1. *Sample-and-Hold*: The design constraints for the input sample-and-hold draws parallel to the design requirements of a high-speed time-interleaved ADC [78]. Different interleaver configurations can be analyzed based on a simplified switch model in which the switch resistance and capacitance are linked to the technology. To reduce effect of sampling jitter, it is preferable to sample first followed by subsampling however at the cost of additional source followers which can significantly impact power consumption and linearity. To relax the power consumption, the first sampler can be interleaved (typically by 2 or 4) at the cost of slightly higher mismatch and jitter [79].

2. *Signal Combiners*: The signal combiner is a critical component for wideband discrete-time beamforming that requires careful design considerations of several parameters including gain, bandwidth, number of summing channels (each channel refers

to a downconverted RF signal from each antenna element), dynamic range, and power consumption. The multi-parameter optimization considering the required design specifications for each system can

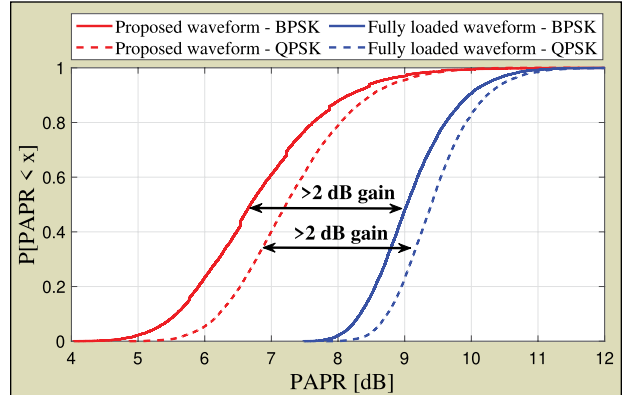


Figure 14. PAPR comparison between proposed and fully loaded OFDM waveforms, assuming BPSK or QPSK symbols.

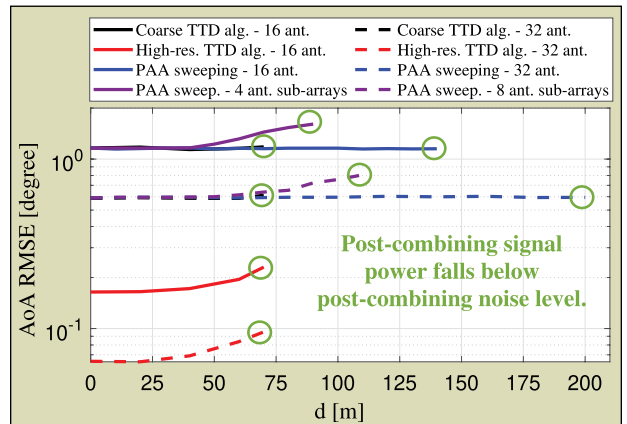


Figure 15. Comparison between TTD algorithms and PAA-based beam sweeping in terms of the AoA RMSE at different distances between the BS and UE.

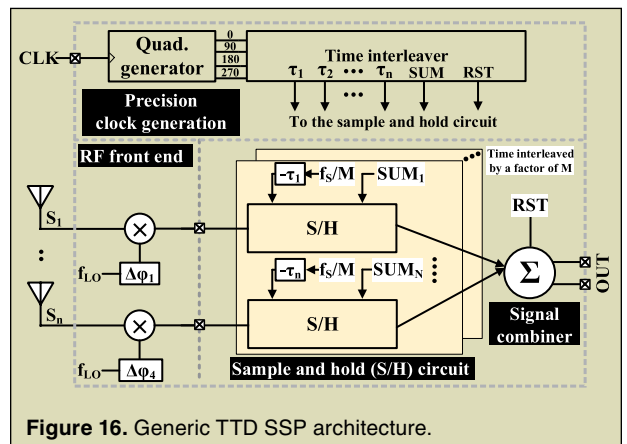


Figure 16. Generic TTD SSP architecture.

be addressed using either a closed-loop or open-loop summing amplifiers, shown in Fig. 17(a). In [22], a closed-loop operational transconductance amplifier (OTA) is used whose design complexity and power consumption are scaled exponentially with the bandwidth. To support larger bandwidths and higher number of antennas, a closed loop integrator using ring amplifier [80], [81] was demonstrated in [26]. Ring amplifiers are technology scalable lending them good candidates to beamform signals from even larger number of antenna elements. In contrast to closed-loop amplifiers, summing can also be performed through daisychain linked voltage-to-time converter (VTC)s as shown in Fig. 17(b). The serialized VTCs each acting in open-loop is digitized by a multi-bit time-to-digital converter (TDC) creating an equivalent of matrix-multiplying ADC.

3. *Precision Clock Generation:* The required sampling phases of the discrete-time SSP can be generated on-chip as illustrated in [22], [26]. To achieve higher precision and matching following Nyquist criterion as well as use the same architecture for different SSP modes, the clock gen-

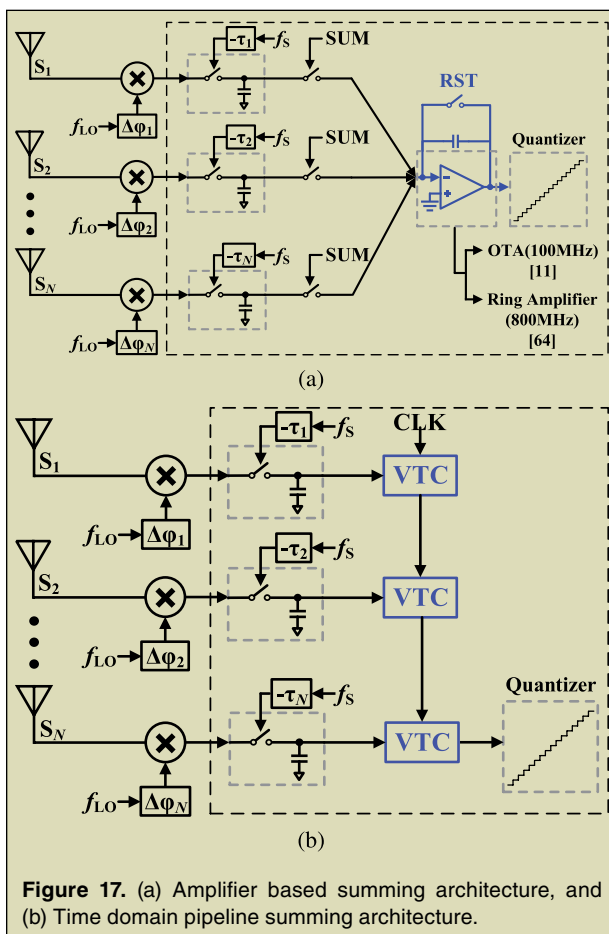


Figure 17. (a) Amplifier based summing architecture, and (b) Time domain pipeline summing architecture.

eration requires N low-power precision phase interpolator (PI) and time-interleavers [22], [51], [52]. The time-interleaver output is applied to interleaved multiply-and-accumulate units that enables them to span the required delay range while meeting the Nyquist bandwidth.

High precision linear PSs are desired to meet the delay range and resolution requirements for the switched-capacitor array as discussed in Section III. Recent works have demonstrated PIs as digital-to-phase generator in different applications including clock-and-data recovery [82], [83] and outphasing transmitters [84], [85]. In general, several architectures have been proposed to implement PI which generates output of phases of weighted sum of two input clock phases based on the digital input code.

The underlying concept of PI can be studied from [86] which describes the process as addition of two phase-shifted edges to produce a new edge with the transition in between them. The output is a superposition of two exponential curves formed by the merged driver output resistance and the capacitive load. The linearity of the PI not only depends on the time difference between the input signals but also their rise times. It has been observed that the non-linearity for a step input response is more whereas it is less for the inputs with finite rise time inputs.

The current-steering digital-to-analog converter (DAC) have been popular architectures for implementing PI [87]. However, the linearity and resolution are greatly impacted by the DAC. As mentioned above, to generate finite rise time at the input, a slew rate control buffer is implemented which requires additional power. The summation of the direct in-phase and quadrature-phase however causes nonlinearity with respect to the codes. Alternatively, current-mode logic based PI architectures can be adopted if the inputs are sinusoidal signals. Instead of interpolating between two consecutive quadrature phases, it can be done in multiple cascaded stages. Interpolation between signals with small phase differences ($<45^\circ$) is more linear than direct interpolation between the quadrature inputs. Though the current-mode logic based PI has lower swing which consumes less dynamic power, it suffers from linearity issue whereas the inverter-based PIs suffers from high dynamic power. Additionally, the PI's output gets affected by the power supply variations. Low-dropout regulators can be applied between the main power supply and the PI supply to alleviate this issue. As such, its important to consider the design trade-offs for N PIs specifically linearity and power consumption.

B. Multi-Antenna Testbed and Validation

Another important step in the design process is developing the test interface between the mmW front-end and

the BB TTD SSP as well as the digital back-end. The wide modulated bandwidths and the large number of down-converted channels from mmW to baseband due to both differential and quadrature configurations challenges the signal generation and post-processing. In addition, all the channels should be synchronized in time with picosecond accuracies to enable efficient data communications. Fig. 18 shows a sample closedloop testbed for 800MHz TTD SSP recently demonstrated in [26]. High speed DACs and

ADCs in ZCU RFSoc family make it possible to generate wideband signals from DACs and perform data capture from the high speed ADC through the same graphic user interface control which serves both as an arbitrary waveform generator and spectrum analyzer in [22]. In [26], 800MHz modulated bandwidth with 16 synchronized channels was generated and the outputs post-processed after digitization in MATLAB offline.

Besides synchronization and large number of channels, repeated parameterized sweeps across frequencies and angles to characterize a multi-antenna transceiver undertakes significant efforts without closed-loop automation in place. In [23], the TTD SSP (in particular, TDC and the time amplifiers) were optimized using particle swarm optimization techniques from [88]. While the optimization was limited to TDC only and not the entire SSP, this method shows the potential opportunities to further extend the test bench automation for closed-loop signal path optimization.

In their recent work, the authors have used computer vision techniques for testbed automation in [89]. These techniques reduces the strenuous manual calibration and test process significantly and enables generation of data-intensive 3D plots (Fig. 19(a)) and frequency-angular maps (Fig. 19(b)) that can be used to create accurate dictionaries for calibration in data communications mode. The shown plots represent 72 individual configurations when the 4-element array is configured to -45° with 500MHz modulated bandwidth at the input. The measured half-power beamwidth is close to the theoretical estimated 35° . Similar map can be generated

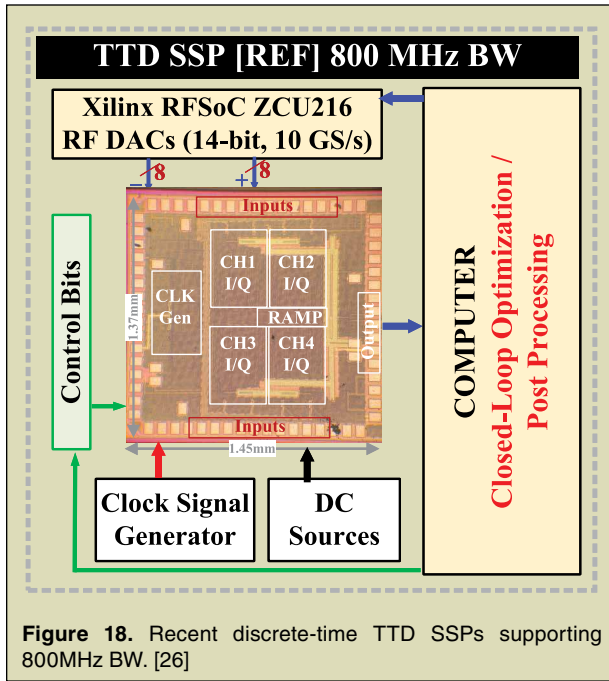


Figure 18. Recent discrete-time TTD SSPs supporting 800MHz BW. [26]

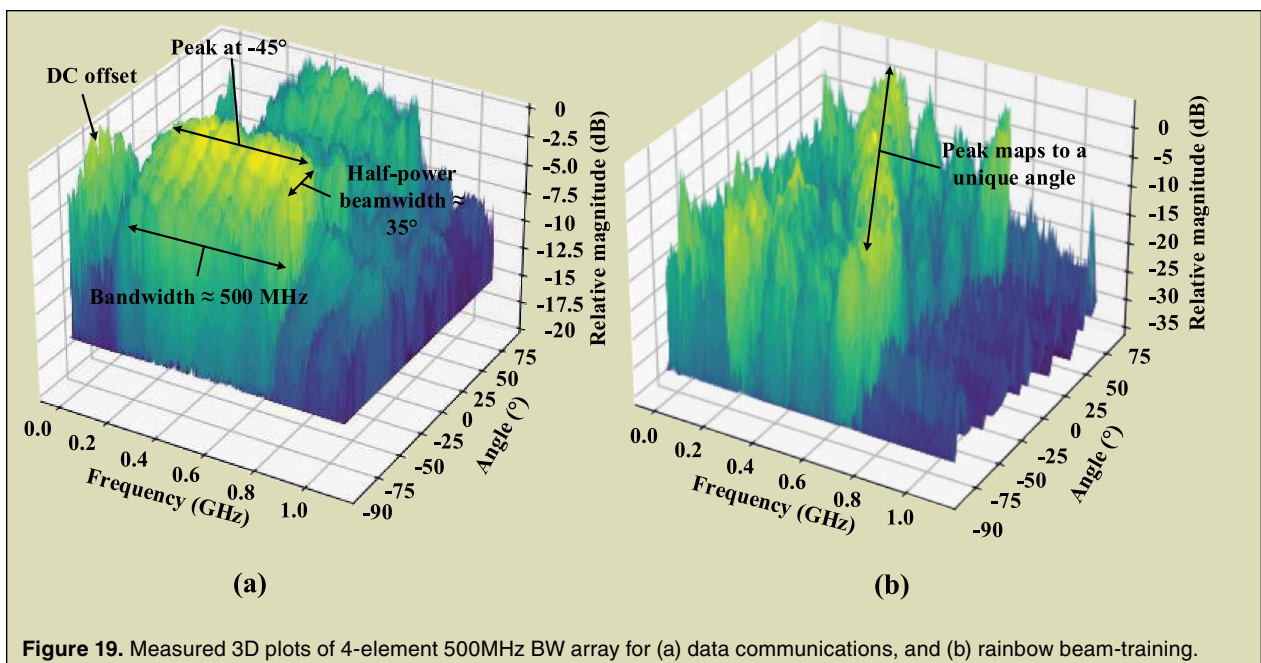


Figure 19. Measured 3D plots of 4-element 500MHz BW array for (a) data communications, and (b) rainbow beam-training.

TTD arrays and their rainbow codebooks can be leveraged to spatially allocate a small fraction of frequency resources to each served user.

for the rainbow beam-training as shown in Fig. 19(b) which shows the efficacy of the proposed algorithm. Additional measurement details for these plots are captured in [89]. The automated test process further minimizes the human errors in the manual process. In addition, this enables benchmarking entire system from the antenna to the higher network layers combined with machine learning algorithms in future.

VI. Future Work

A. 3D Rainbow Beam with Planar TTD Array

In principle, the frequency dependent beam steering can be extended into the planar TTD array. In our recent work [90] we studied beamforming codebooks with the uniform delay steps $\Delta\tau_x, \Delta\tau_y$, introduced in the antenna elements in the x-y plane before combining, i.e., the received signal in the (i,j) -th element is delayed by $(i-1)\Delta\tau_x + (j-1)\Delta\tau_y$. We showed that uniform delay spacing can create 3D beams such that different frequency components are steered toward a unique spherical direction (θ, ϕ) . Further, the entire 3D angular space can be covered by at least one beam. Fig. 20 presents the frequency dispersing steering for 10 frequency components. However, this preliminary study also reveals a number of design challenges from both circuits and system perspectives. On the one hand, the required maximum delay range is increased. For planar array with a total N elements, the required delay range

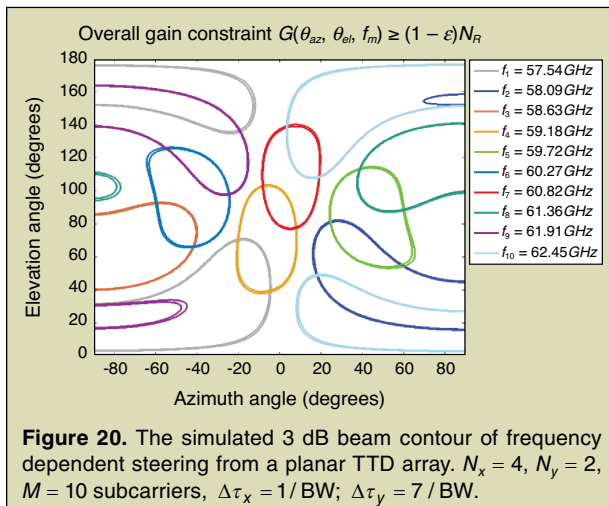
is at least $2(N-1)/BW$, a factor of 2 larger than its linear array counterpart. On the other hand, as compared to the rainbow beam using a linear TTD array, the 3D rainbow beam using planar array has some unique characteristics. More specifically, beams from some frequency component experience a reduced gain as compared to others. There is non-trivial challenge to calibrate the beam pattern and design beam training algorithm tailored for this non-ideality.

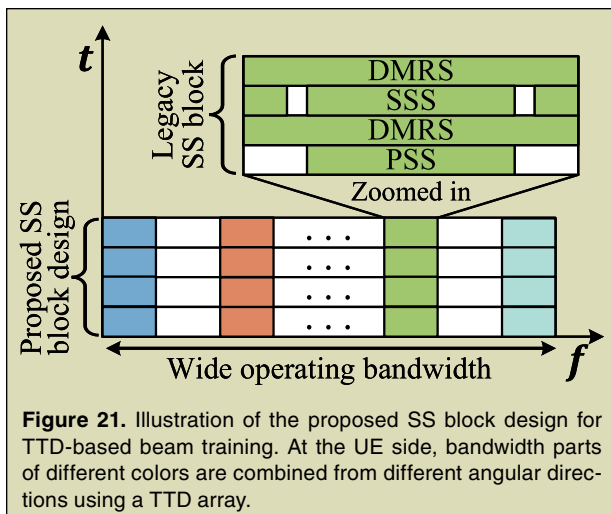
B. TTD Rainbow Beam Enabled Multiple Access

Beam training is not the only application of the TTD array dispersive rainbow beam. In [91], a novel orthogonal frequency division multiple access scheme was proposed. In low-mobility line-of-sight scenarios, TTD arrays and their rainbow codebooks can be leveraged to spatially allocate a small fraction of frequency resources to each served user. There are a number of advantages that make such scheme appealing for the future IoT application. Firstly, the hardware bandwidth of each user can be much smaller than that of the infrastructure. This facilitates a power- and cost-friendly design for the terminals. Secondly, the conventional time division beam switching can be eliminated, because different users are simultaneously served using different frequency resources, which are allocated based on the corresponding rainbow beam directions. It is worth noting that the frequency-to-angle mapping in rainbow codebooks is deterministic, i.e., TTD arrays cannot independently tune frequencies to arbitrary angles. However, it is possible to exploit phase shifters in different RF chains of TTD arrays to rotate the entire mapping and enable the spatial reuse of frequencies. The TTD-based massive access scheme can also reduce the beam management overhead to support IoT applications with strict latency requirements [91]. To this end, designing a frame structure and synchronization procedure that are compatible with existing standard represents one of the most important challenges.

C. Compatibility of TTD Beam Training with 5G Standard

Exhaustive beam sweeping with synchronization is the main part of the IA procedure in 5G New Radio Standard. It is performed using periodic bursts of up to 64SS blocks, each associated with a different steering





direction [56]. An SS block is a group of 4 consecutive OFDM symbols with 240 subcarriers (20 resource blocks) that carry the Primary Synchronization Signal (PSS), Secondary Synchronization Signal (SSS), and DeModulation Reference Signal (DMRS). The PSS and SSS are leveraged for synchronization between the BS and UE, while the DMRS can be used to estimate the received power associated with that direction, i.e., SS block.

Since the proposed TTD beam training is fundamentally different from beam sweeping, its compatibility with the current 5G New Radio Standard becomes an important problem. In our preliminary work, we proposed a different design of the SS block, which exploits wide available bandwidth at mmW frequencies and supports TTD beam training, as illustrated in Fig. 21. In the proposed design, the existing reference signals are repeated multiple times across the operating bandwidth. With such training waveform, the UE is capable of receiving at least one entire legacy SS block using its frequency-dependent beam steering. The UE can then leverage DSP to extract the reference signals to achieve synchronization with the BS and determine the best steering direction. The proposed SS block design removes the need for SS bursts and thus minimizes the required overhead in TTD beam training. However, the design depends on different system parameters, including the number of subcarriers, number of UE antennas, and resolution of UE beam probing. We plan to address these practical design questions in our future work.

VII. Conclusion

Reconfigurable TTD arrays are essential for emerging mmW wireless communications demanding wide bandwidths with ultra-low-latency in direction finding

compared to current wireless standards. This magazine article presents a comprehensive overview of the recent developments in TTD arrays enabling multiple SSP functions. Delay compensation techniques are exploited to prevent beam squint during data communications while introducing intentional beam squint for fast beam-training. The article combines the beam-training algorithm with the underlying architectural and circuit design considerations. The exciting developments in TTD arrays presented herein lays out a future path for enabling next-generation network and physical infrastructure wireless solutions on a large-scale with 3D direction finding for communications-on-the-move applications, massive machine type communications, and standardization in emerging wireless standards.

Acknowledgment

The authors would like to thank Ruifu Li from UCLA for his help in preparing the manuscript.



Chung-Ching Lin (Graduate Student Member, IEEE) received the M.S. degree in communication engineering from Yuan Ze University, Taoyuan, Taiwan, in 2014. He is currently pursuing the Ph.D. degree with Washington State University, Pullman, WA, USA. His current research interests include low power and wideband multi-antenna transceivers, frequency synthesizer, and high-speed I/O circuit design. He was a recipient of the Yu-Ziang Academic Scholarship in 2013, the Southern Methodist University Graduate Student Travel Grant in 2018, the IEEE Circuits and Systems Society (CAS) Travel Award in 2019, and the IEEE Custom Integrated Circuits Conference (CICC) Educational Grants Award in 2020. He was the IEEE Radio Frequency Integrated Circuits (RFIC) Symposium Best Student Paper Award Nominee (out of 12 finalists) in 2020.



Veljko Boljanovic (Graduate Student Member, IEEE) received the B.S. and M.S. degrees in electrical and computer engineering from the University of Novi Sad, Novi Sad, Serbia, in 2015 and 2016, respectively. He is currently pursuing the Ph.D. degree with the University of California at Los Angeles, Los Angeles, CA, USA. His research interests include system design, network performance optimization, and digital signal processing in wireless millimeter-wave communications. He was a recipient of the Electrical and Computer Engineering Department Fellowship and the Dissertation Year Fellowship at the University of California at Los Angeles in 2017 and 2021, respectively.



Han Yan (Graduate Student Member, IEEE) received the B.E. degree from Zhejiang University, Hangzhou, China, in 2013, and the M.S. and Ph.D. degrees in electrical and computer engineering from UCLA in 2015 and 2020, respectively. His research interests include signal processing and communication system design for millimeter-wave mobile networks, cooperative unmanned aerial vehicles networks, and dynamic spectrum sharing radios. He was a recipient of the UCLA Dissertation Year Fellowship in 2018, Qualcomm Innovation Fellowship in 2019, UCLA ECE Distinguished Ph.D. Dissertation Award in 2020, and the Best Paper Award at the 2020 ACM mmNets Workshop.



Erfan Ghaderi (Member, IEEE) received the B.Sc. degree in electrical engineering from the Sharif University of Technology, Tehran, Iran, in 2012, the M.Sc. degree in circuits and systems from the University of Tehran, Tehran, in 2015, and the Ph.D. degree from the School of Electrical Engineering and Computer Science, Washington State University, Pullman, WA, USA, in 2020. He is currently an Analog Design Engineer with Intel Corporation, Hillsboro, OR, USA. His research interests include integrated circuit design for high-speed data converters, phased array applications, and time-domain signal processing.



Mohammad Ali Mokri (Graduate Student Member, IEEE) received the B.Sc. degree in electrical engineering from the Hamedan University of Technology, Hamedan, Iran, in 2012, and the M.Sc. degree from the University of Tehran, Tehran, in 2015. He is currently pursuing the Ph.D. degree with Washington State University, Pullman, WA, USA. His research interests include integrated circuit design for phased array applications, mm-wave transmitters, and power amplifiers. He also serves as a Reviewer for IEEE MICROWAVE AND WIRELESS COMPONENTS LETTERS.



Jayce Jeron Gaddis (Student Member, IEEE) received the dual B.S. degrees (*summa cum laude*) in electrical engineering and computer engineering from Washington State University, Pullman, WA, USA, in 2021. He currently works as an Electrical Design Engineer with Cadence Neuroscience, Redmond, WA, developing analog/mixed signal systems for next-generation medical devices. His research interests include signal processing, medical electronics, and analog/mixed signal circuit design.



Aditya Wadaskar (Graduate Student Member, IEEE) received the B.Tech. and M.Tech. degrees in electrical engineering from the Indian Institute of Technology Madras, Chennai, India, in 2020. He is currently pursuing the Ph.D. degree with the University of California at Los Angeles, Los Angeles, CA, USA. His research interests include beam training and interference suppression in wireless millimeter wave communication.



Chase Puglisi (Member, IEEE) received the B.S. and M.S. degrees from Washington State University (WSU) in 2017 and 2020, respectively. While he was working towards his M.S., he worked with the Systems-on-Chip (SoC) Laboratory, WSU. He currently works as an Analog Design Engineer at Texas Instruments, Tucson, AZ, USA. His research interests include time-based circuits, hybrid amplifier design, and multi-channel phased array systems.



Soumen Mohapatra (Graduate Student Member, IEEE) received the B.S. degree in electrical engineering from the National Institute of Technology (NIT), Rourkela, India, in 2015. He is currently pursuing the Ph.D. degree with Washington State University, Pullman, WA, USA. Prior to that, he was working with the CMOS Image Sensor Group, ON Semiconductor, India, for two years, and Power Management IC Team, Samsung Research and Development, India, for two years. His research interests include design of frequency synthesizers, switched inductor capacitor voltage regulator, and mixed signal circuit design.



Qiuyan Xu (Graduate Student Member, IEEE) received the B.E. degree in electronic science and technology from Xi'an Jiaotong University, Xi'an, China, in 2017, and the M.S. degree in electrical engineering from Washington State University, Pullman, WA, USA, in 2019, where she is currently pursuing the Ph.D. degree. Her research interests include time-domain circuits, high-speed mixed-signal designs, and applications in wireless communication systems.



Sreeni Poolakkal (Graduate Student Member, IEEE) received the B.Tech. degree from the University of Calicut, Calicut, in 2014, and the M.Tech. degree from the IIT Guwahati, Guwahati, India, in 2018. He is currently pursuing the

Ph.D. degree with Washington State University, Pullman, WA, USA. He did his master's thesis on low-power and low phase noise oscillators.

Subsequently, he joined Tata Steel, Jamshedpur, India, as an Automation Technologist. His research interests include highly linear and wideband phased array radios. He was a recipient of the IEEE Solid-State Circuits Society (SSCS), Student Travel Grant Award (STGA) to attend International Solid State Circuits Conference (ISSCC) 2022.



Deukhyoun Heo (Senior Member, IEEE) received the B.S. degree in electrical engineering from Kyungpuk National University, South Korea, in 1989, the M.S. degree in electrical engineering from the Pohang University of Science

and Technology (POSTECH), Pohang, South Korea, in 1997, and the Ph.D. degree in electrical and computer engineering from the Georgia Institute of Technology, Atlanta, GA, USA, in 2000. In 2000, he joined National Semiconductor Corporation, where he was a Senior Design Engineer. In the fall of 2003, he joined the Faculty of Electrical Engineering and Computer Science Department, Washington State University, Pullman, WA, USA, where he is currently the Frank Brands Analog Distinguished Professor of electrical engineering. He has authored or coauthored approximately 165 publications, including 80 peer-reviewed journal articles and 85 international conference papers. His research interests include mm-wave/sub-THz transceiver for wireless and wireline data communications, wireless sensors and power management systems, beamformers for phased-array communications, and low-power wireless links for biomedical applications. He has been a member of the Technical Committee of the IEEE Microwave Theory and Techniques Society (IEEE MTT-S). He was a recipient of the 2000 Best Student Paper Award presented at the IEEE MTT-S IMS and the 2009 National Science Foundation (NSF) Career Award. He has served as an Associate Editor for the IEEE TRANSACTIONS ON CIRCUITS AND SYSTEMS—II: EXPRESS BRIEFS and the IEEE TRANSACTIONS ON MICROWAVE THEORY AND TECHNIQUES. He is also serving as an Associate Editor for the IEEE TRANSACTIONS ON VERY LARGE SCALE INTEGRATION (VLSI) SYSTEMS and the IEEE MICROWAVE AND WIRELESS COMPONENTS LETTERS.



Subhanshu Gupta (Senior Member, IEEE) received the B.E. degree from the National Institute of Technology (NIT), Tiruchirappalli, India, in 2002, and the M.S. and Ph.D. degrees from the University of Washington in 2006

and 2010, respectively.

He is currently an Associate Professor of electrical engineering and computer science at Washington State University. He has held industrial positions at Maxlinear, Irvine, CA, USA, where he worked on wideband transceivers for SATCOM and infrastructure applications. His research interests include large-scale phased arrays and wideband transceivers, low-power time-domain circuits and systems, statistical hardware optimization for next-generation wireless communications, the Internet of Things, and cryo-electronics. He was a recipient of the National Science Foundation Career Award in 2019, the Department of Defense DURIP Award in 2020, and the Cisco Faculty Research Award in 2017. He has received the Analog Devices Outstanding Student Designer Award in 2008 and the IEEE RFIC Best Student Paper Award (3rd place) in 2011. He serves as an Associate Editor for the IEEE TRANSACTIONS ON CIRCUITS AND SYSTEMS—I: REGULAR PAPERS for the term 2020–2023 and a Technical Program Committee for IEEE RFIC since 2022.



Danijela Cabric (Fellow, IEEE) received the M.S. degree in electrical engineering from the University of California at Los Angeles (UCLA), Los Angeles, CA, USA, in 2001, and the Ph.D. degree in electrical engineering

from the UC Berkeley in 2007. She is currently a Professor of electrical and computer engineering at the University of California at Los Angeles, Los Angeles, CA, USA. Her research interests include millimeter-wave communications, distributed communications and sensing for the Internet of Things, and machine learning for wireless networks co-existence and security. She received the Samuelli Fellowship in 2008, the Okawa Foundation Research Grant in 2009, the Hellman Fellowship in 2012, the National Science Foundation Faculty Early Career Development (CAREER) Award in 2012, and the Qualcomm Faculty Award in 2020. She served as an Associate Editor for the IEEE TRANSACTIONS ON COGNITIVE COMMUNICATIONS AND NETWORKING, IEEE TRANSACTIONS ON WIRELESS COMMUNICATIONS, IEEE TRANSACTIONS ON MOBILE COMPUTING, and *IEEE Signal Processing Magazine*, and as a IEEE ComSoc Distinguished Lecturer.

References

- [1] A. Ghosh et al., "Millimeter-wave enhanced local area systems: A high-data-rate approach for future wireless networks," *IEEE J. Sel. Areas Commun.*, vol. 32, no. 6, pp. 1152–1163, Jun. 2014.
- [2] T. S. Rappaport et al., "Millimeter wave mobile communications for cellular: It will work!" *IEEE Access*, vol. 1, pp. 335–349, 2013.
- [3] R. Baldemair et al., "Ultra-dense networks in millimeter-wave frequencies," *IEEE Commun. Mag.*, vol. 53, no. 1, pp. 202–208, Jan. 2015.
- [4] N. Bhusan et al., "Network densification: The dominant theme for wireless evolution into 5G," *IEEE Commun. Mag.*, vol. 52, no. 2, pp. 82–89, Feb. 2014.

- [5] V. Raghavan et al., "Millimeter-wave MIMO prototype: Measurements and experimental results," *IEEE Commun. Mag.*, vol. 56, no. 1, pp. 202–209, Jan. 2018.
- [6] Y. Huang et al., "Multi-panel MIMO in 5G," *IEEE Commun. Mag.*, vol. 56, no. 3, pp. 56–61, Mar. 2018.
- [7] R. W. Heath, Jr., et al., "An overview of signal processing techniques for millimeter wave MIMO systems," *IEEE J. Sel. Topics Signal Process.*, vol. 10, no. 3, pp. 436–453, Apr. 2016.
- [8] H. Shokri-Ghadikolaei et al., "Millimeter wave cellular networks: A MAC layer perspective," *IEEE Trans. Commun.*, vol. 63, no. 10, pp. 3437–3458, Oct. 2015.
- [9] P. Yang et al., "6G wireless communications: Vision and potential techniques," *IEEE Netw.*, vol. 33, no. 4, pp. 70–75, Jul. 2019.
- [10] Z. Zhang et al., "6G wireless networks: Vision, requirements, architecture, and key technologies," *IEEE Veh. Technol. Mag.*, vol. 14, no. 3, pp. 28–41, Sep. 2019.
- [11] R. Rotman, M. Tur, and L. Yaron, "True time delay in phased arrays," *Proc. IEEE*, vol. 104, no. 3, pp. 504–518, Mar. 2016.
- [12] T.-S. Chu, J. Roderick, and H. Hashemi, "An integrated ultra-wideband timed array receiver in 0.13 μm CMOS using a path-sharing true time delay architecture," *IEEE J. Solid-State Circuits*, vol. 42, no. 12, pp. 2834–2850, Dec. 2007.
- [13] H. Hashemi, T.-S. Chu, and J. Roderick, "Integrated true-time-delay-based ultra-wideband array processing," *IEEE Commun. Mag.*, vol. 46, no. 9, pp. 162–172, Sep. 2008.
- [14] T. Chu and H. Hashemi, "True-time-delay-based multi-beam arrays," *IEEE Trans. Microw. Theory Techn.*, vol. 61, no. 8, pp. 3072–3082, Aug. 2013.
- [15] S. Garakoui et al., "Compact cascaded g m -C all-pass true-time-delay cell with reduced delay variation over frequency," *IEEE J. Solid-State Circuits*, vol. 50, no. 3, pp. 693–703, Mar. 2015.
- [16] F. Hu and K. Mouthaan, "A 1–20 GHz 400 ps true-time delay with small delay error in 0.13 μm CMOS for broadband phased array antennas," in *IEEE MTT-S Int. Microw. Symp. Dig.*, May 2015, pp. 1–3.
- [17] M.-K. Cho, I. Song, and J. D. Cressler, "A true time delay-based SiGe bi-directional T/R chipset for large-scale wideband timed array antennas," in *Proc. IEEE Radio Freq. Integr. Circuits Symp. (RFIC)*, Jun. 2018, pp. 272–275.
- [18] S. Jang et al., "A true time delay 16-element 4-beam digital beamformer," in *Proc. IEEE Radio Freq. Integr. Circuits Symp. (RFIC)*, Jun. 2018, pp. 12–15.
- [19] S. Mondal et al., "A 25–30 GHz fully-connected hybrid beamforming receiver for MIMO communication," *IEEE J. Solid-State Circuits*, vol. 53, no. 5, pp. 1275–1287, May 2018.
- [20] S. Jang et al., "A 1-GHz 16-element four-beam true-time-delay digital beamformer," *IEEE J. Solid-State Circuits*, vol. 54, no. 5, pp. 1304–1314, May 2019.
- [21] M. B. Dastjerdi et al., "28.6 full-duplex 2x2 MIMO circulator-receiver with high TX power handling exploiting MIMO RF and shared-delay baseband self-interference cancellation," in *IEEE Int. Solid-State Circuits Conf. (ISSCC) Dig. Tech. Papers*, Feb. 2019, pp. 448–450.
- [22] E. Ghaderi et al., "An integrated discrete-time delay-compensating technique for large-array beamformers," *IEEE Trans. Circuits Syst. I, Reg. Papers*, vol. 66, no. 9, pp. 3296–3306, Sep. 2019.
- [23] E. Ghaderi et al., "A 4-element 500 MHz-modulated-BW 40 mW 6b 1 GS/s analog-time-to-digital-converter-enabled spatial signal processor in 65 nm CMOS," in *IEEE Int. Solid-State Circuits Conf. (ISSCC) Dig. Tech. Papers*, Feb. 2020, pp. 186–188.
- [24] K. Spoof et al., "A 0.6–4.0 GHz RF-resampling beamforming receiver with frequency-scaling true-time-delays up to three carrier cycles," *IEEE Solid-State Circuits Lett.*, vol. 3, pp. 234–237, 2020.
- [25] E. Ghaderi and S. Gupta, "A four-element 500-MHz 40-mW 6-bit ADC-enabled time-domain spatial signal processor," *IEEE J. Solid-State Circuits*, vol. 56, no. 6, pp. 1784–1794, Jun. 2021.
- [26] C.-C. Lin et al., "A 4-element 800 MHz-BW 29 mW true-time-delay spatial signal processor enabling fast beam-training with data communications," in *Proc. IEEE 47th Eur. Solid State Circuits Conf. (ESSCIRC)*, Sep. 2021, pp. 287–290.
- [27] J. Paramesh et al., "A four-antenna receiver in 90-nm CMOS for beamforming and spatial diversity," *IEEE J. Solid-State Circuits*, vol. 40, no. 12, pp. 2515–2524, Dec. 2005.
- [28] A. Hajimiri et al., "Integrated phased array systems in silicon," *Proc. IEEE*, vol. 93, no. 9, pp. 1637–1655, Sep. 2005.
- [29] A. Natarajan, A. Komijani, and A. Hajimiri, "A fully integrated 24-GHz phased-array transmitter in CMOS," *IEEE J. Solid-State Circuits*, vol. 40, no. 12, pp. 2502–2514, Dec. 2005.
- [30] A. Natarajan et al., "A 77-GHz phased-array transceiver with on-chip antennas in silicon: Transmitter and local lo-path phase shifting," *IEEE J. Solid-State Circuits*, vol. 41, no. 12, pp. 2807–2819, Dec. 2006.
- [31] S. Jeon et al., "A scalable 6-to-18 GHz concurrent dual-band quad-beam phased-array receiver in CMOS," *IEEE J. Solid-State Circuits*, vol. 43, no. 12, pp. 2660–2673, Dec. 2008.
- [32] H. Krishnaswamy and H. Hashemi, "A 4-channel 4-beam 24-to-26 GHz spatio-temporal RAKE radar transceiver in 90 nm CMOS for vehicular radar applications," in *IEEE Int. Solid-State Circuits Conf. (ISSCC) Dig. Tech. Papers*, Feb. 2010, pp. 214–215.
- [33] A. Valdes-Garcia et al., "A fully integrated 16-element phased-array transmitter in SiGe BiCMOS for 60-GHz communications," *IEEE J. Solid-State Circuits*, vol. 45, no. 12, pp. 2757–2773, Dec. 2010.
- [34] M. C. M. Soer et al., "Spatial interferer rejection in a four-element beamforming receiver front-end with a switched-capacitor vector modulator," *IEEE J. Solid-State Circuits*, vol. 46, no. 12, pp. 2933–2942, Dec. 2011.
- [35] A. Natarajan et al., "A fully-integrated 16-element phased-array receiver in SiGe BiCMOS for 60-GHz communications," *IEEE J. Solid-State Circuits*, vol. 46, no. 5, pp. 1059–1075, May 2011.
- [36] M. Soer et al., "A 1.5-to-5.0 GHz input-matched +2 dBm P_{1dB} all-passive switched-capacitor beamforming receiver front-end in 65 nm CMOS," in *IEEE Int. Solid-State Circuits Conf. (ISSCC) Dig. Tech. Papers*, Feb. 2012, pp. 174–176.
- [37] A. Ghaffari et al., "A 4-element phased-array system with simultaneous spatial- and frequency-domain filtering at the antenna inputs," *IEEE J. Solid-State Circuits*, vol. 49, no. 6, pp. 1303–1316, Jun. 2014.
- [38] H. Krishnaswamy and L. Zhang, "Analog and RF interference mitigation for integrated MIMO receiver arrays," *Proc. IEEE*, vol. 104, no. 3, pp. 561–575, Mar. 2016.
- [39] L. Zhang, A. Natarajan, and H. Krishnaswamy, "Scalable spatial notch suppression in spatio-spectral-filtering MIMO receiver arrays for digital beamforming," *IEEE J. Solid-State Circuits*, vol. 51, no. 12, pp. 3152–3166, Dec. 2016.
- [40] L. Zhang and H. Krishnaswamy, "Arbitrary analog/RF spatial filtering for digital MIMO receiver arrays," *IEEE J. Solid-State Circuits*, vol. 52, no. 12, pp. 3392–3404, Dec. 2017.
- [41] M.-Y. Huang et al., "An all-passive negative feedback network for broadband and wide field-of-view self-steering beam-forming with zero DC power consumption," *IEEE J. Solid-State Circuits*, vol. 52, no. 5, pp. 1260–1273, May 2017.
- [42] M. Johnson et al., "A 4-element 28 GHz millimeter-wave MIMO array with single-wire interface using code-domain multiplexing in 65 nm CMOS," in *Proc. IEEE Radio Freq. Integr. Circuits Symp. (RFIC)*, Jun. 2019, pp. 243–246.
- [43] M.-Y. Huang and H. Wang, "A 27-to-41 GHz MIMO receiver with N-input-N-output using scalable cascaded autonomous array-based high-order spatial filters for instinctual full-FoV multi-blocker/signal management," in *IEEE Int. Solid-State Circuits Conf. (ISSCC) Dig. Tech. Papers*, Feb. 2019, pp. 346–348.
- [44] M.-Y. Huang and H. Wang, "A mm-wave wideband MIMO RX with instinctual array-based blocker/signal management for ultralow-latency communication," *IEEE J. Solid-State Circuits*, vol. 54, no. 12, pp. 3553–3564, Dec. 2019.
- [45] S. Mondal and J. Paramesh, "A reconfigurable 28-/37-GHz MMSE-adaptive hybrid-beamforming receiver for carrier aggregation and multi-standard MIMO communication," *IEEE J. Solid-State Circuits*, vol. 54, no. 5, pp. 1391–1406, May 2019.
- [46] I. Mondal and N. Krishnapura, "A 2-GHz bandwidth, 0.25–1.7 ns true-time-delay element using a variable-order all-pass filter architecture in 0.13 μm CMOS," *IEEE J. Solid-State Circuits*, vol. 52, no. 8, pp. 2180–2193, Aug. 2017.
- [47] B. Wang et al., "Spatial- and frequency-wideband effects in millimeter-wave massive MIMO systems," *IEEE Trans. Signal Process.*, vol. 66, no. 13, pp. 3393–3406, Jul. 2018.

- [48] M. Cai, "Modeling and mitigating beam squint in millimeter wave wireless communication," Ph.D. dissertation, Dept. Elect. Eng, Univ. Notre Dame, Notre Dame, IN, USA, 2018.
- [49] B. Wang et al., "Spatial-wideband effect in massive MIMO with application in mmWave systems," *IEEE Commun. Mag.*, vol. 56, no. 12, pp. 134–141, Dec. 2018.
- [50] X. Liu and D. Qiao, "Space-time block coding-based beamforming for beam squint compensation," *IEEE Wireless Commun. Lett.*, vol. 8, no. 1, pp. 241–244, Feb. 2019.
- [51] V. Boljanovic et al., "Fast beam training with true-time-delay arrays in wideband millimeter-wave systems," *IEEE Trans. Circuits Syst. I, Reg. Papers*, vol. 68, no. 4, pp. 1727–1739, Apr. 2021.
- [52] E. Ghaderi et al., "Four-element wide modulated bandwidth MIMO receiver with >35-dB interference cancellation," *IEEE Trans. Microw. Theory Techn.*, vol. 68, no. 9, pp. 3930–3941, Sep. 2020.
- [53] R. J. Mailloux, *Phased Array Antenna Handbook*, 2nd ed. Boston, MA, USA: Artech House, Mar. 2005.
- [54] *Electromagnetic Waves and Antennas*. Accessed: Apr. 10, 2022. [Online]. Available: <https://www.ece.rutgers.edu/~orfanidi/ewa/>
- [55] H. Yan and D. Cabric, "Compressive initial access and beamforming training for millimeter-wave cellular systems," *IEEE J. Sel. Topics Signal Process.*, vol. 13, no. 5, pp. 1151–1166, Sep. 2019.
- [56] M. Giordani et al., "A tutorial on beam management for 3GPP NR at mmWave frequencies," *IEEE Commun. Surveys Tuts.*, vol. 21, no. 1, pp. 173–196, 1st Quart., 2018.
- [57] C. Jeong, J. Park, and H. Yu, "Random access in millimeter-wave beamforming cellular networks: Issues and approaches," *IEEE Commun. Mag.*, vol. 53, no. 1, pp. 180–185, Jan. 2015.
- [58] J. Kim and A. F. Molisch, "Fast millimeter-wave beam training with receive beamforming," *J. Commun. Netw.*, vol. 16, no. 5, pp. 512–522, Oct. 2014.
- [59] K. Hosoya et al., "Multiple sector ID capture (MIDC): A novel beamforming technique for 60-GHz band multi-Gbps WLAN/PAN systems," *IEEE Trans. Antennas Propag.*, vol. 63, no. 1, pp. 81–96, Jan. 2015.
- [60] L. Zhou and Y. Ohashi, "Efficient codebook-based MIMO beamforming for millimeter-wave WLANs," in *Proc. IEEE 23rd Int. Symp. Pers., Indoor Mobile Radio Commun. (PIMRC)*, Sep. 2012, pp. 1885–1889.
- [61] H. Yan, V. Boljanovic, and D. Cabric, "Wideband millimeter-wave beam training with true-time-delay array architecture," in *Proc. 53rd Asilomar Conf. Signals, Syst., Comput.*, Nov. 2019, pp. 1447–1452.
- [62] M. Sayginer and G. M. Rebeiz, "An eight-element 2–16-GHz programmable phased array receiver with one, two, or four simultaneous beams in SiGe BiCMOS," *IEEE Trans. Microw. Theory Techn.*, vol. 64, no. 12, pp. 4585–4597, Dec. 2016.
- [63] A. Nafe et al., "2×64-element dual-polarized dual-beam single-aperture 28-GHz phased array with 2×30 Gb/s links for 5G polarization MIMO," *IEEE Trans. Microw. Theory Techn.*, vol. 68, no. 9, pp. 3872–3884, Sep. 2020.
- [64] B. Sadhu et al., "A 28-GHz 32-element TRX phased-array IC with concurrent dual-polarized operation and orthogonal phase and gain control for 5G communications," *IEEE J. Solid-State Circuits*, vol. 52, no. 12, pp. 3373–3391, Dec. 2017.
- [65] J. D. Dunworth et al., "A 28 GHz bulk-CMOS dual-polarization phased-array transceiver with 24 channels for 5G user and basestation equipment," in *IEEE Int. Solid-State Circuits Conf. (ISSCC) Dig. Tech. Papers*, Feb. 2018, pp. 70–72.
- [66] J. Pang et al., "A 28-GHz CMOS phased-array transceiver based on LO phase-shifting architecture with gain invariant phase tuning for 5G new radio," *IEEE J. Solid-State Circuits*, vol. 54, no. 5, pp. 1228–1242, May 2019.
- [67] Y. Wang et al., "A 39-GHz 64-element phased-array transceiver with built-in phase and amplitude calibrations for large-array 5G NR in 65-nm CMOS," *IEEE J. Solid-State Circuits*, vol. 55, no. 5, pp. 1249–1269, May 2020.
- [68] G. Mangraviti et al., "A 4-antenna-path beamforming transceiver for 60 GHz multi-Gb/s communication in 28 nm CMOS," in *IEEE Int. Solid-State Circuits Conf. (ISSCC) Dig. Tech. Papers*, Jan. 2016, pp. 246–247.
- [69] S. Pellerano et al., "A scalable 71-to-76 GHz 64-element phased-array transceiver module with 2×2 direct-conversion IC in 22 nm FinFET CMOS technology," in *IEEE Int. Solid-State Circuits Conf. (ISSCC) Dig. Tech. Papers*, Feb. 2019, pp. 174–176.
- [70] B. Yang et al., "Digital beamforming-based massive MIMO transceiver for 5G millimeter-wave communications," *IEEE Trans. Microw. Theory Techn.*, vol. 66, no. 7, pp. 3403–3418, Jul. 2018.
- [71] A. Nagulu et al., "A full-duplex receiver with true-time-delay cancelers based on switched-capacitor-networks operating beyond the delay–bandwidth limit," *IEEE J. Solid-State Circuits*, vol. 56, no. 5, pp. 1398–1411, May 2021.
- [72] X. Guan, H. Hashemi, and A. Hajimiri, "A fully integrated 24-GHz eight-element phased-array receiver in silicon," *IEEE J. Solid-State Circuits*, vol. 39, no. 12, pp. 2311–2320, Dec. 2004.
- [73] Y. Ghasempour et al., "Single shot single antenna path discovery in THz networks," in *Proc. 26th Annu. Int. Conf. Mobile Comput. Netw.* New York, NY, USA: Association for Computing Machinery, Apr. 2020, pp. 1–13, doi: 10.1145/3372224.3380895.
- [74] J. Tan and L. Dai, "Wideband beam tracking in THz massive MIMO systems," *IEEE J. Sel. Areas Commun.*, vol. 39, no. 6, pp. 1693–1710, Jun. 2021.
- [75] V. Boljanovic et al., "Design of millimeter-wave single-shot beam training for true-time-delay array," in *Proc. IEEE 21st Int. Workshop Signal Process. Adv. Wireless Commun. (SPAWC)*, May 2020, pp. 1–5.
- [76] 5GPPP. (May 2017). *Measurement Results and Final mmMAGIC Channel Models*. [Online]. Available: <http://5g-mmmagic.eu>
- [77] L. Kull et al., "A 24–72-GS/s 8-b time-interleaved SAR ADC with 2.0–3.3-pJ/conversion and SNDR at Nyquist in 14-nm CMOS FinFET," *IEEE J. Solid-State Circuits*, vol. 53, no. 12, pp. 3508–3516, Dec. 2018.
- [78] Y. M. Greshishchev et al., "A 40 GS/s 6b ADC in 65 nm CMOS," in *IEEE Int. Solid-State Circuits Conf. (ISSCC) Dig. Tech. Papers*, Feb. 2010, pp. 390–391.
- [79] B. Hershberg et al., "A 61.5 dB SNDR pipelined ADC using simple highly-scalable ring amplifiers," in *Proc. Symp. VLSI Circuits (VLSIC)*, Jun. 2012, pp. 32–33.
- [80] B. Hershberg et al., "Ring amplifiers for switched capacitor circuits," *IEEE J. Solid-State Circuits*, vol. 47, no. 12, pp. 2928–2942, Dec. 2012.
- [81] M.-T. Hsieh and G. Sobelman, "Architectures for multi-gigabit wire-linked clock and data recovery," *IEEE Circuits Syst. Mag.*, vol. 8, no. 4, pp. 45–57, 4th Quart., 2008.
- [82] M. Y. He and J. Poulton, "A CMOS mixed-signal clock and data recovery circuit for OIF CEI-6G+ backplane transceiver," *IEEE J. Solid-State Circuits*, vol. 41, no. 3, pp. 597–606, Mar. 2006.
- [83] Y.-H. Liu and T.-H. Lin, "A wideband PLL-based G/FSK transmitter in 0.18 μm CMOS," *IEEE J. Solid-State Circuits*, vol. 44, no. 9, pp. 2452–2462, Sep. 2009.
- [84] P.-E. Su and S. Pamarti, "A 2.4 GHz wideband open-loop GFSK transmitter with phase quantization noise cancellation," *IEEE J. Solid-State Circuits*, vol. 46, no. 3, pp. 615–626, Mar. 2011.
- [85] D. Weinlader, "Precision CMOS receivers for VLSI testing applications," Ph.D. dissertation, Stanford Univ., Stanford, CA, USA, Nov. 2001. [Online]. Available: https://vlisweb.stanford.edu/people/alum/pdf/0111_Weinlader_Precision_CMOS_Receivers.pdf
- [86] J. F. Bulzacchelli et al., "A 10-Gb/s 5-tap DFE/4-tap FFE transceiver in 90-nm CMOS technology," *IEEE J. Solid-State Circuits*, vol. 41, no. 12, pp. 2885–2900, Dec. 2006.
- [87] S. Bansal et al., "Neural-network based self-initializing algorithm for multi-parameter optimization of high-speed ADCs," *IEEE Trans. Circuits Syst. II, Exp. Briefs*, vol. 68, no. 1, pp. 106–110, Jan. 2021.
- [88] C.-C. Lin et al., "Multi-mode spatial signal processor with rainbow-like fast beam training and wideband communications using true-time-delay arrays," *IEEE J. Solid-State Circuits*, vol. 57, no. 11, pp. 3348–3360, Nov. 2022, doi: 10.1109/JSSC.2022.3178798.
- [89] A. Wadaskar et al., "3D rainbow beam design for fast beam training with true-time-delay arrays in wideband millimeter-wave systems," in *Proc. 55th Asilomar Conf. Signals, Syst., Comput.*, Oct. 2021, pp. 85–92.
- [90] R. Li, H. Yan, and D. Cabric, "Rainbow-link: Beam-alignment-free and grant-free mmW multiple access using true-time-delay array," *IEEE J. Sel. Areas Commun.*, vol. 40, no. 5, pp. 1692–1705, May 2022.